Task 5. Oxygenates

The objective of this task is to obtain a better understanding of the factors that affects catalyst selectivity toward oxygenates for iron-based Fischer-Tropsch catalysts.

No scheduled activity to report.

Task 6. Literature Review of Prior Fischer-Tropsch Synthesis with Co Catalysts

The objective of this task is to prepare a critical review of prior work on cobalt Fischer-Tropsch catalysts.

Work is continuing on an extensive review of FTS kinetics.

Task 7. Co Catalyst Preparation

The objective of this task is to prepare a limited number of cobalt-based Fischer-Tropsch catalysts that can be used to obtain baseline data on cobalt-based Fischer-Tropsch synthesis.

See Task 8.

Task 8. Cobalt Catalyst Testing for Activity and Kinetic Rate Correlations

The objective of this task is to conduct initial screening of the cobalt catalysts prepared in Task 7 to select three baseline catalysts that will then be used to generate a data base on the performance of cobalt-based Fischer-Tropsch catalysts in slurry reactors.

A. CO and CO_2 Hydrogenation over Co-Pt/Al_2O_3 Catalyst

Introduction

The feed syngas from natural gas contains a small amount of CO_2, the effect of CO_2 therefore should be studied to determine the necessity of separation of CO_2 from syngas. Study of CO_2 hydrogenation will also help us understand the mechanism for methane formation. CO_2 methanation is important in production of substitute natural gas, since it contributes additional methane needed to meet heating value specifications. Two categories of mechanisms for CO_2

hydrogenation has been proposed based on the early work done on nickel catalysts, (1) conversion of CO_2 to CO via the reverse water gas shift reaction followed by CO methanation, and (2) direct hydrogenation of CO_2 to methane by a mechanism distinct form CO methanation.

Previous works on CO and CO_2 hydrogenation of our group leads to the conclusion that CO hydrogenation rate is much higher than CO_2 over cobalt catalyst and CO_2 methanation goes through methanol as an intermediate.

The purpose of this investigation is to determine the deactivation rate for CO_2 hydrogenation at different H_2:CO ratio and different conversion level, as well as the deactivation rate of CO hydrogenation. We would probably have a better understanding of the mechanism of deactivation.

Experimental

Preparation of Co-Pt/Al_2O_3

Condea vista B alumina with a surface area of 300m^2/g, pore volume of 1.15m^3/g was used as support materials and the cobalt loading was 15%. A multi-step incipient wetness impregnation method was used to add cobalt nitrate solution to alumina with a drying procedure after each impregnation at 80^{0}C in a rotary evaporator. Following cobalt addition, tetramineplatinum nitrate solution was e added by an incipient wetness impregnation method and the platinum loading was 0.5%. The catalyst was then dried in a rotary evaporator at 80^{0}C again and calcined at 400^{0}C for 4hrs.

Fixed-bed Fischer-Tropsch Synthesis Study

3g of Co-Pt/Al_2O_3 catalyst was diluted by 15g of glass bead and then loaded in a two inch diameter reactor, a three zone furnace was used to control the temperature of the reactor. Four Brooks mass flow controllers were used to control the flow rate of CO, CO_2, H_2 and He. Fischer-

Tropsch synthesis was conducted at 210^0C, 350psig with H_2:CO=2:1 and GHSV=5.0SL/hr/gcatalyst(H_2:CO:He=2:1:2). CO_2 hydrogenation was tested at same temperature and pressure but with H_2:CO ratio of both 2:1(H_2:CO:He=2:1:2) and 4:1(H_2:CO_2:He=4:1:4). The space velocity was changed from 9.0SL/hr/gcatalyst to 5.0 SL/hr/gcatalyst.

Results and Discussion

Since we use H_2:CO ratio of 2:1 as the feed gas, the highest CO_2 conversion is 50%. At time on stream 48hr, CO_2 conversion observed was 45% which is close to equilibrium. The fact that the conversion decreased at 0.81% CO_2 conversion per day indicated that the catalyst is reasonably stable for CO_2 hydrogenation. In order to investigate the stability of catalyst far from equilibrium, we increased the flow rate from 5.0SL/hr/gcatalyst to 9.0SL/hr/gcatalyst. The deactivation rate became even lower(from 0.81% to 0.69% CO_2 conversion per day) and the activity range maintained at about 20% CO_2 conversion range.

One of the assumptions for the deactivation mechanism of cobalt Fischer-Tropsch synthesis catalyst is the oxidation of surface cobalt to oxide or cobalt aluminate by water. Our assumption of the oxidation mechanism is that when H_2O/H_2 partial pressure ratio goes up to certain point, the oxidation of the cobalt cluster starts to occur. For CO_2 hydrogenation when the conversion level is at 40%, the H_2O/H_2 partial pressure ratio is about 2.0 and is much higher than CO hydrogenation (0.3 at 40% CO conversion). But for CO_2 hydrogenation, the deactivation is not so obvious (figure 1 is the CO_2 conversion as a function of time on stream). One explanation is that the oxidation only occurs to the small clusters and the methanation of CO_2 is catalyzed by the larger cobalt clusters. The other explanation is that the surface oxidation did not occur as fast as CO hydrogenation. That makes the assumption of H_2O/H_2 partial pressure ratio as the decisive factor for the oxidation invalid. It also brings up another explanation of the deactivation of CO

hydrogenation, which is H_2O/CO ratio is a more important factor. One possibility is that the adsorption of H_2O and CO are competitive and since more H_2O has been formed, the less CO can been adsorbed. But the results of CO_2 hydrogenation eliminate that possibility; therefore, one can conclude that H_2O and CO has formed some kind of intermediate which caused the oxidation or crystal growth of cobalt clusters.

Since the methanation of CO_2 requires H_2:CO ratio of 4:1, we adjusted the feed gas to this ratio to further study the stability of the catalyst and the results are shown in figure 2. When the conversion level is 42%, the catalyst did not deactivate after 24hrs, then the flow rate was decreased to achieve a conversion of about 55%; the catalyst started to deactivate slowly but leveled off at about 40% CO_2 conversion. It can been concluded that during CO_2 hydrogenation, deactivation is slower than for CO hydrogenation even at high conversion levels.

After 504 hours of using CO_2 as a feed gas, CO hydrogenation was studied with a H_2:CO ratio of 2:1 and space velocity of 5SL/hr/gcatalyst. Figure 3 shows the results of CO conversion as a function of time on stream, and figure 4 is CO and CO_2 conversion as a function of time on stream when CO was used as the feed gas first. It can been concluded that CO_2 hydrogenation did cause deactivation of the catalyst for subsequent CO hydrogenation since, after 504 hours of time on stream, CO conversion decreased from 52.5% to 28.7%. However, it can been seen from figure 3 that the deactivation rate of CO hydrogenation is much faster than CO_2 hydrogenation at 30% CO conversion. If the feed gas is CO and the conversion is 60%, the deactivation rate could have been much higher and after 504 hours of time on stream, CO conversion rate would have been much lower than 28.7%. From figure 3, it seems that the CO conversion stayed at about 20% and it agrees with our CSTR data that the deactivation rate is a function of CO conversion level; the lower the CO conversion, the lower the deactivation rate.

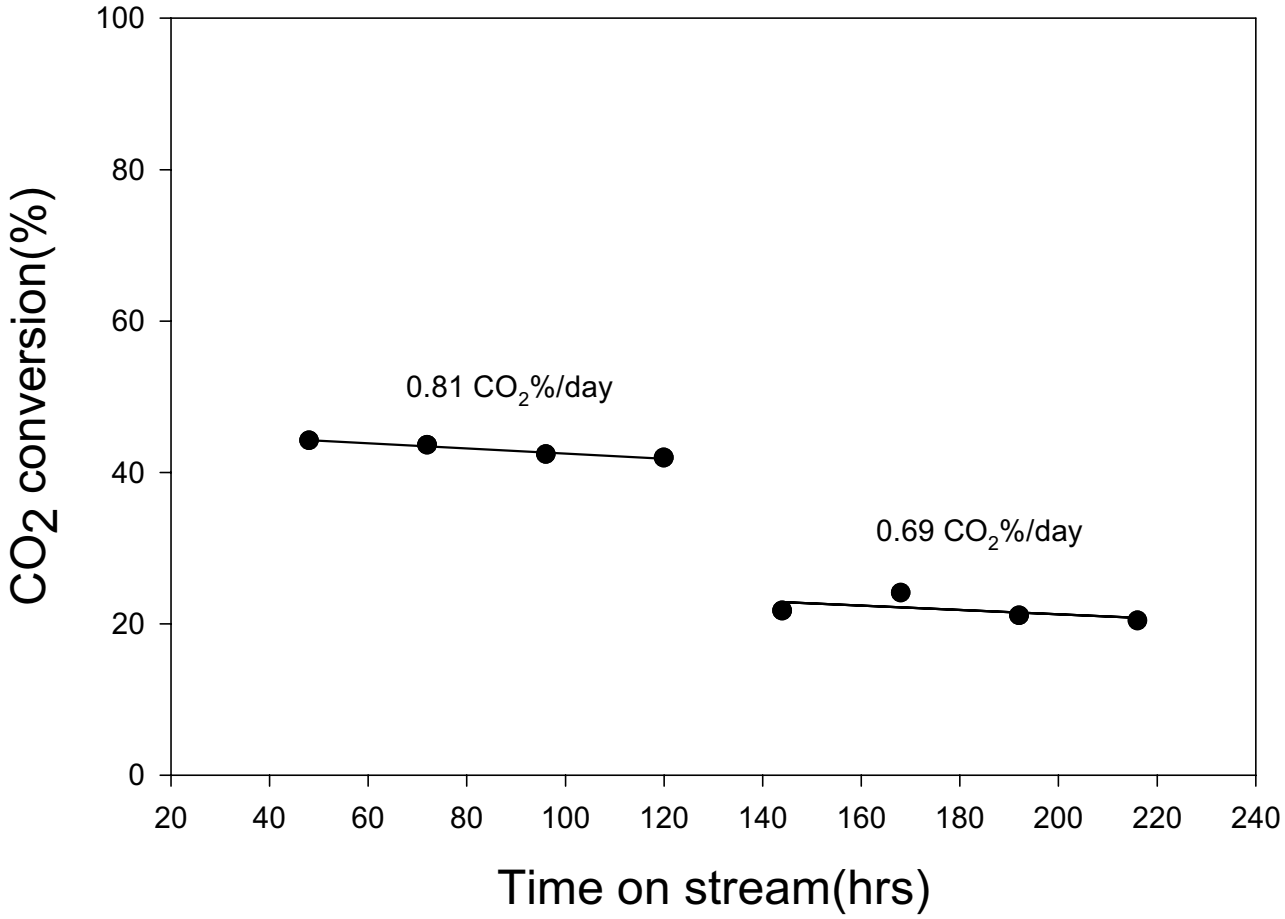

Figure 1. CO_2 hydrogenation over Co-Pt/Al_2O_3, 210^oC, 350psig, H_2:CO=2:1, GHSV=5.0SL/hr/gcatalyst.

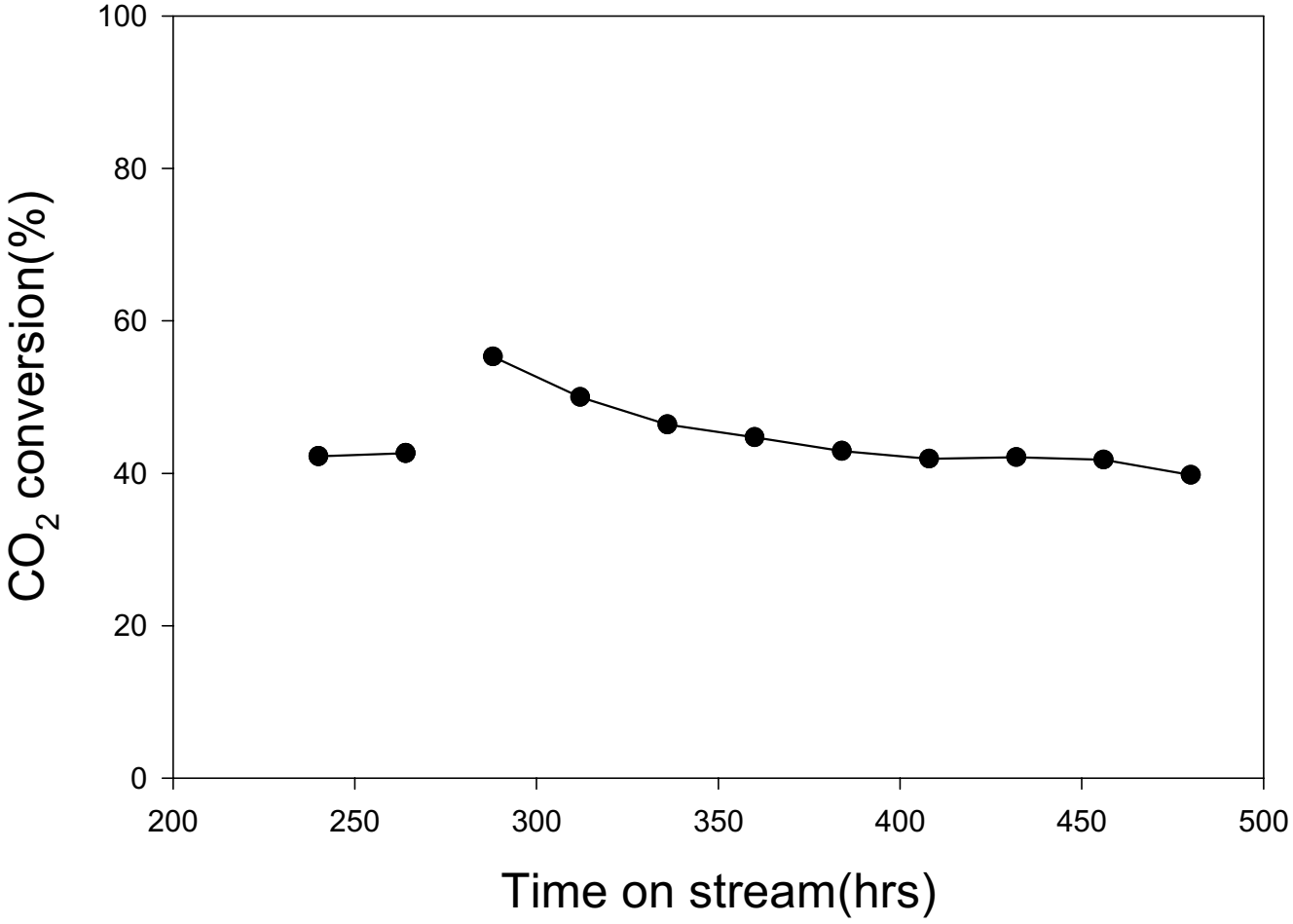

Figure 2. CO_2 hydrogenation over Co-Pt/Al_2O_3 at 210^oC, 350psig, H_2:CO=4:1, GHSV=9.0 and 5.0SL/hr/gcatalyst.

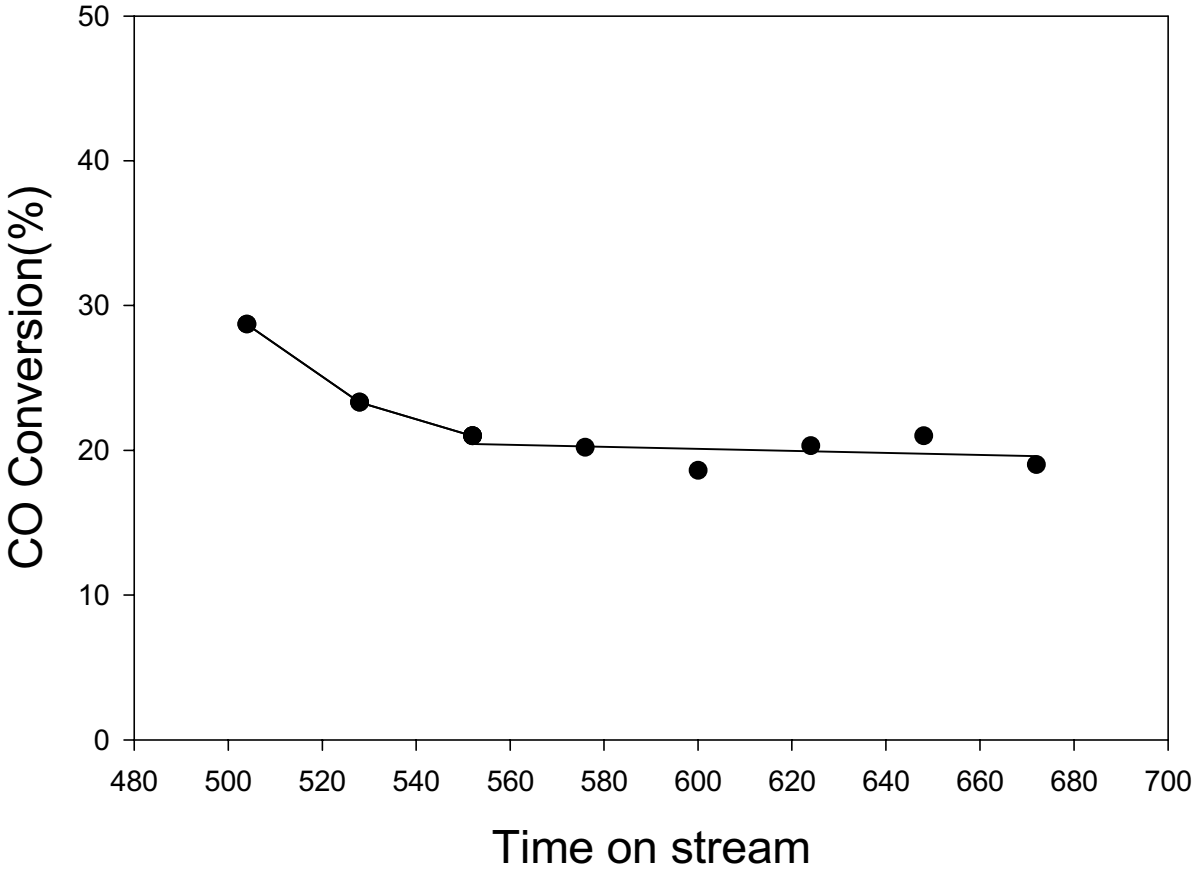

Figure 3. CO hydrogenation over Co-Pt/Al_2O_3 at 210^oC, 350psig, H_2:CO=2:1, GHSV=5.0SL/hr/gcatalyst.

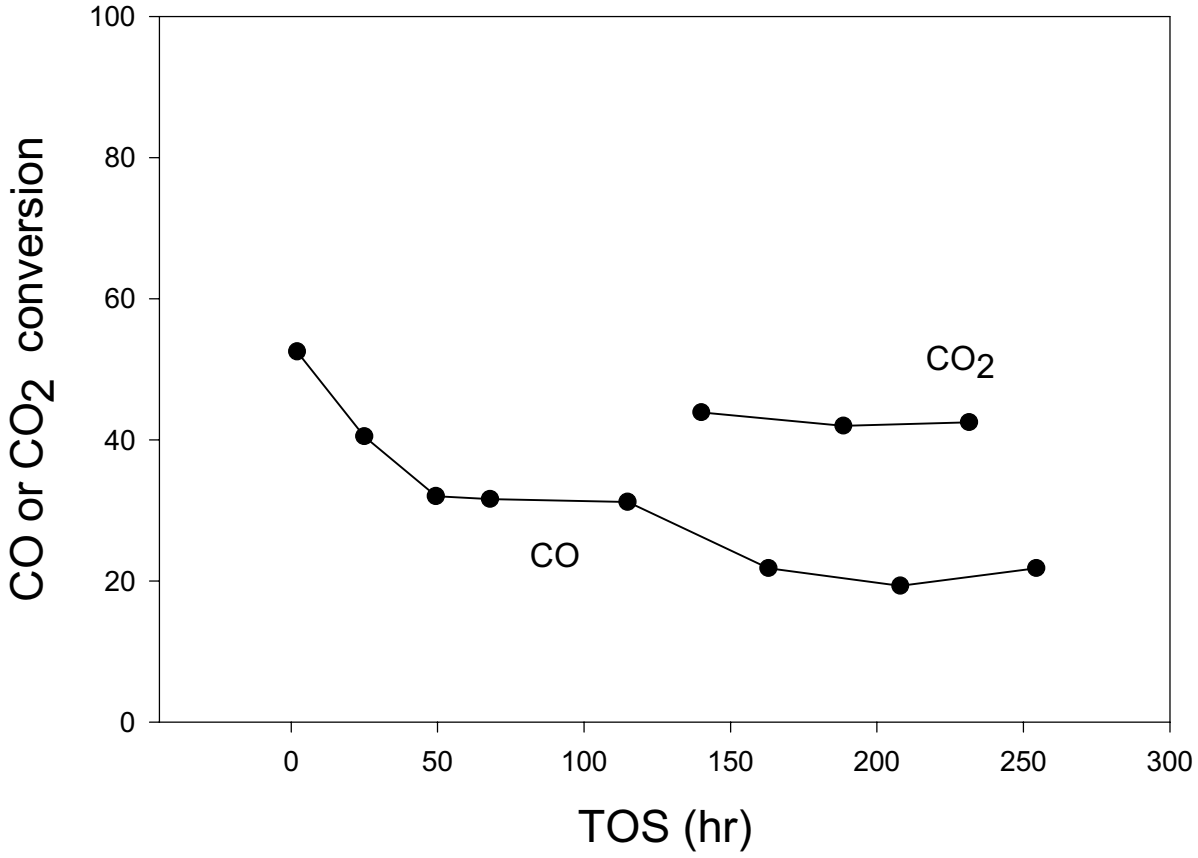

Figure 4. CO or CO_2 conversion as a function of time on stream

Task 9. Cobalt Catalyst Life Testing

The objective of this task is to obtain life data on baseline cobalt Fischer-Tropsch catalysts.

A. Deactivation Rates for Co Catalysts

Introduction

In comparison with low cost Fe FTS catalysts, cobalt catalysts may work at relatively low reaction temperatures and pressures with higher yields of linear paraffins in the C_{5+} range and do not convert water by water gas shift reaction. The cobalt catalysts are believed to deactivate less than the Fe-based catalyst. The major drawback of cobalt catalyst is it high cost. Therefore, the present studies focused on improving the deactivation rates of these catalysts.

Experimental

Preparation of Cobalt Catalysts

The Co/Al_2O_3 catalyst was prepared by incipient wetness impregnation of Al_2O_3 (Condea Vista B alumina, BET surface area 200 m^2/g, pore volume 0.4 cm^3/g) with cobalt nitrate solution. The preparation procedure includes three step impregnations of cobalt salt and then followed by impregnation of promoter. Finally, calcined the sample at 400°C in the flow Air and Helium.

Pretreatment of the catalysts

The catalysts were pretreated first ex-situ and then in-situ, according to the following procedure. The catalysts were reduced ex-situ using 30% H_2 and 70% He (V/V) in a fixed bed reactor at a space velocity of 10,000 GHSV at 350°C. The temperature was ramped to 350°C at 1°C/min and held at 350°C for 10 hours. This reduced catalysts were transferred to CSTR in inert atmosphere. This was accomplished by over pressuring the fixed bed reactor that contain the reduced catalyst and then opening the appropriate valves to force the entire catalyst volume

into the CSTR containing startup solvent. The reduction reactor was weighed prior to and after catalyst transfer to ensure that a quantitative transfer of catalyst had been accomplished. The catalyst was then reduced in-situ in the CSTR; the hydrogen was introduced to reactor at atmospheric pressure with the flow rate of 30 SL/hr. The reactor temperature was increased to 230°C at the ramp rate 1°C for 12 hours.

Reaction conditions

Approximately 20 g of catalyst was transfer into a 1 liter stirred autoclave which had been charged with 300 g of C_{30} oil(decene trimer obtained from Ethyl Corp.). The catalyst was reduced at 230°C in-situ in atmospheric pressure for 10 hours in the flow of hydrogen. After reduction, the reactor temperature was lowered to 180°C and synthesis gas was introduced into the reactor. Then the reactor was pressurized to 275 psig and temperature was slowly increased to 220°C during 3 hours. The feed gas used in the reaction was H_2 : CO ratio of 2:1.

Results and Discussion

Unpromoted 15%Co/Al_2O_3 catalysts

The activity and rate of loss of activity of the unpromoted Co/Al_2O_3 catalyst are shown in Fig. 1. The initial CO conversion, at space velocity 5 SL/hr/g catalyst, is 18%. The deactivation rate of unpromoted Co/Al_2O_3 catalyst is low (1.56% CO conversion/week) compared to Re or Ru promoted catalysts.

FT-Kinetic Studies of 15%Co/Al_2O_3 Catalysts

Typically, the activity of the fresh catalyst decreases with time on stream and then levels off in 5-7 days. After this period, the deactivation is slow and linear. The kinetic study was performed during the steady state. Two sets of kinetic studies were carried out with constant CO partial pressure (table 1) and constant H_2 partial pressure (table 2). Four H_2/CO ratios and five

space velocities has been used to determine the rates. Argon gas used as the makeup gas to adjust the space velocity. The CO conversion with different space time at different H_2/CO ratio presented in Fig. 2 and Fig. 3. However, the additional calculations are required to determine the reaction rate and that will be done during the next quarter.

To determine the Activation Energy, we have carried out FT runs at four temperatures. The Arhenius plots are presented in Fig. 4 and Fig. 5. The activation energy, calculated from CO conversion and H_2 conversion from Figs. 4 and 5, respectively, is approximately 17 Kcal/mole in both cases.

Pressure Effect over 0.2%Re-15%Co/Al_2O_3 catalyst

The effect pressure on CO conversion of the 0.2%-Re-15%Co/Al_2O_3 and space velocity 2 SL/hr/ g catalyst is shown in Fig. 6. The CO conversion increases with increasing pressure. The CO conversion increased significantly from 100 psig to 300 psig. The effect of pressure on methane selectivity and CO_2 selectivity is shown in Fig. 7. The methane selectivity decreases slightly with increase in pressure but the CO_2 selectivity remain almost same with increases in pressure.

Activity of 0.5%Ru-15%Co/Al_2O_3 and 0.5%Ru-20%Co/ZrO_2-SiO_2 Catalysts

The objective of this task is to find the stable Co-based Fischer-Tropsch catalysts. In this study, our aim was to determine the effect of support to the deactivation rate of the catalyst in comparison with the unpromoted Co/Al_2O_3 catalyst. The activities of 0.5%Ru-15%Co/Al_2O_3 and 0.5%Ru-20%Co/ZrO_2-SiO_2 Catalysts are shown in Fig. 8 and Fig. 9, respectively. Initial CO conversion of 0.5%Ru-15%Co/Al_2O_3 catalyst is two times greater than the initial activity of unpromoted 15%Co/Al_2O_3 catalyst at a space velocity of 5 SL/hr/g. However, the rate of deactivation is greater for the promoted Ru catalyst. While for the unpromoted catalyst, the CO

conversion dropped by 18% of the initial activity after 85 h, and remained stable after that, the CO conversion dropped by 42% of the initial value after 1000 h for the Ru promoted catalyst. The activity of Ru-promoted ZrO_2-SiO_2 catalyst also showed a higher activity than the unpromoted catalyst. However, the deactivation rate is lower (3.53% CO conversion/week) than for the Ru-promoted Al_2O_3 catalyst (4.2% CO conversion/week) at space velocity of 5 SL/hr/g. Similar studies are continuing .

Activity of 0.5%Pt-15%Co/Al_2O_3 Catalyst

The activity tests performed in CST and Fixed-bed reactor are presented in Fig. 10 and Fig.11, respectively. The initial activity of Pt-catalyst is about the same as the Ru-promoted catalyst at space velocity 5 SL/hr/g. The CO conversion in the fixed-bed reactor at 210°C is ~30.0% after 500 hrs time on stream (Fig. 11).

Table 1 : Inlet gas composition for the kinetic studies (constant CO partial pressure)

H_2/CO ratio	1.0	1.5	2.0	2.4
CO%	25	25	25	25
H_2%	25	37.5	50	60
Ar%	50	37.5	25	15

Table 2 : Inlet gas composition for the Kinetic studies (constant H2 partial pressure)

H_2/CO ratio	1.0	1.5	2.0	2.4
CO%	25	16.7	12.5	10.4
H_2%	25	25	25	25
Ar%	50	58.3	62.5	64.6

Fig. 1 : Time on Stream vs CO conversion over Co/Al_2O_3 at 220°C and 275 psig

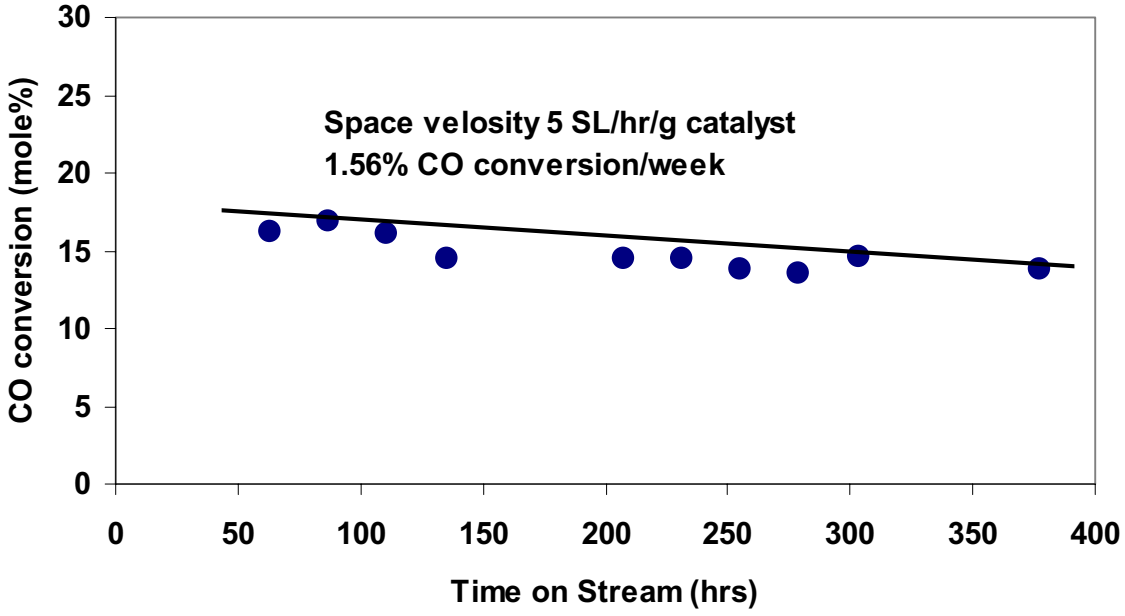

Fig. 2 : Kinetic of 15%Co/Al_2O_3 at 220°C and 275 psig pressure (constant CO partial press.)

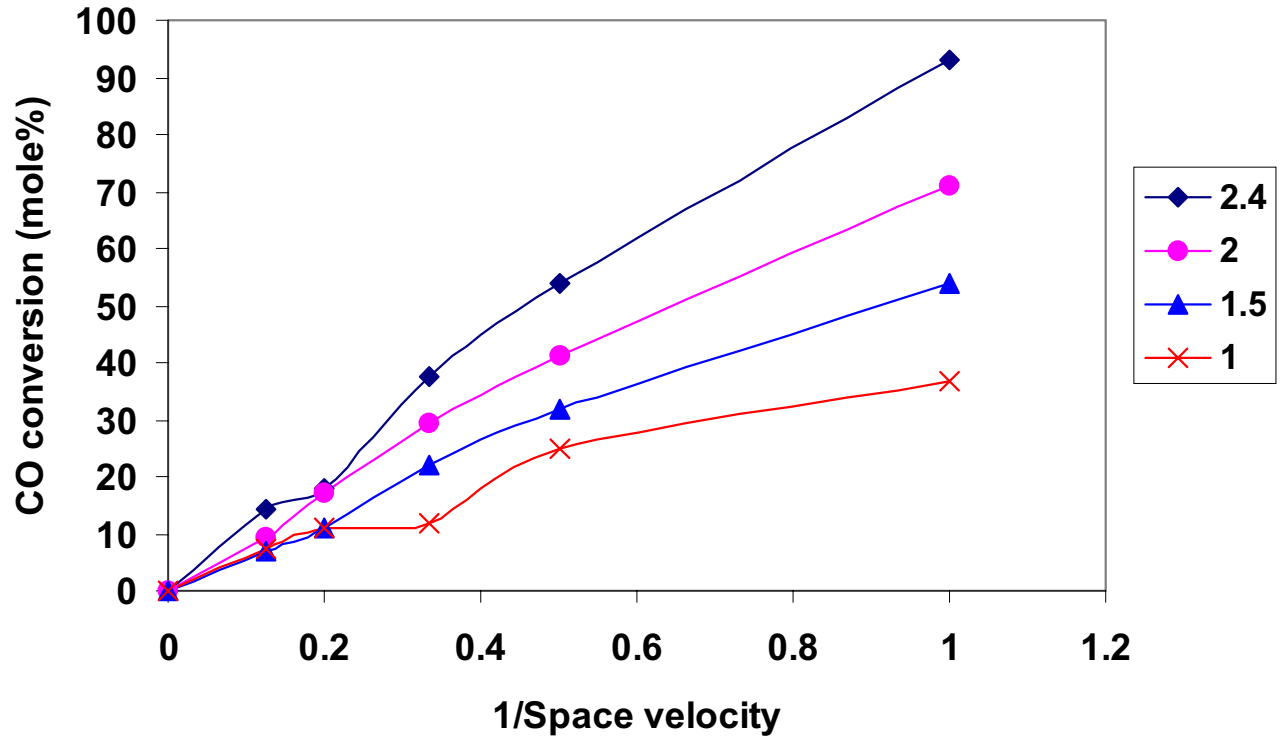

Fig. 3 : Kinetic of CO/Al_2O_3 catalyst at 220°C and 275 psig pressure (contant H_2 partial Press.)

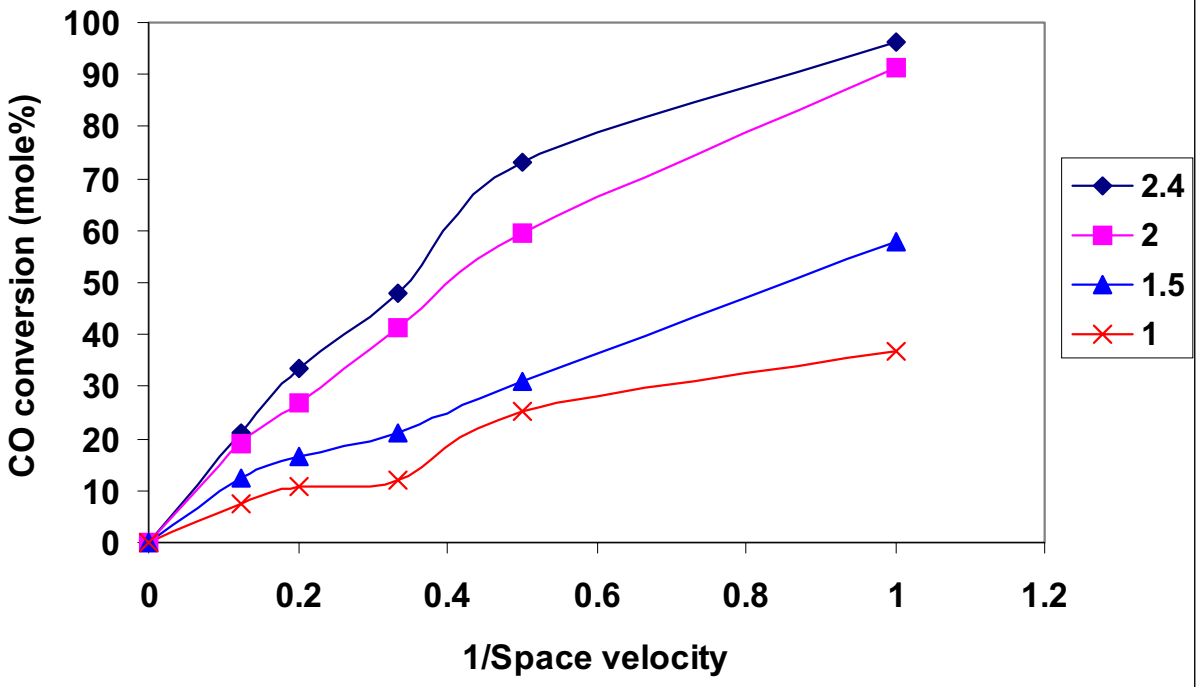

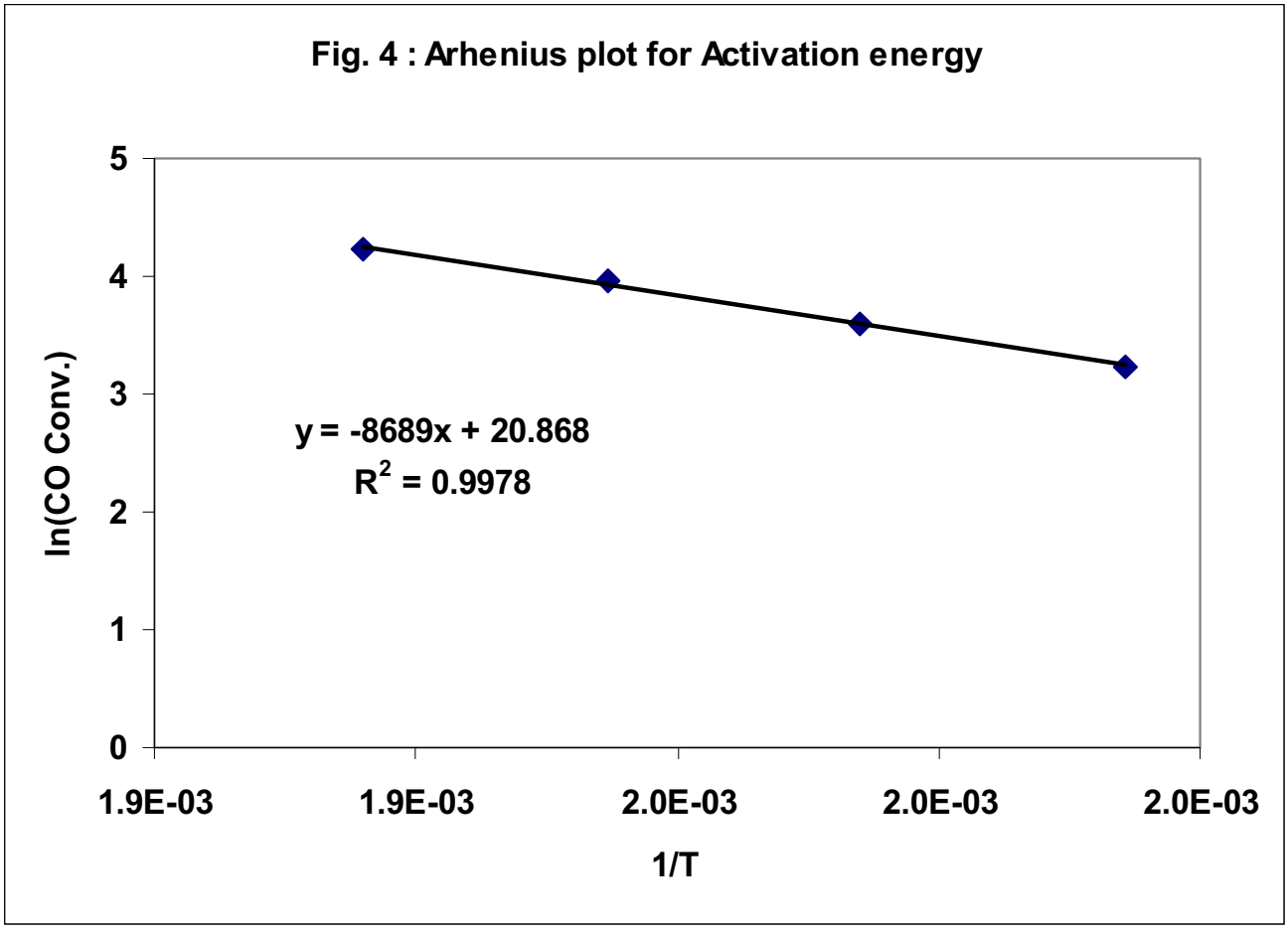
Fig. 4 : Arhenius plot for Activation energy
5
4
3
2
1
0
ln(CO Conv.)
y = -8689x + 20.868
R2 = 0.9978
1.9E-03
1.9E-03
2.0E-03
2.0E-03
2.0E-03
1/T

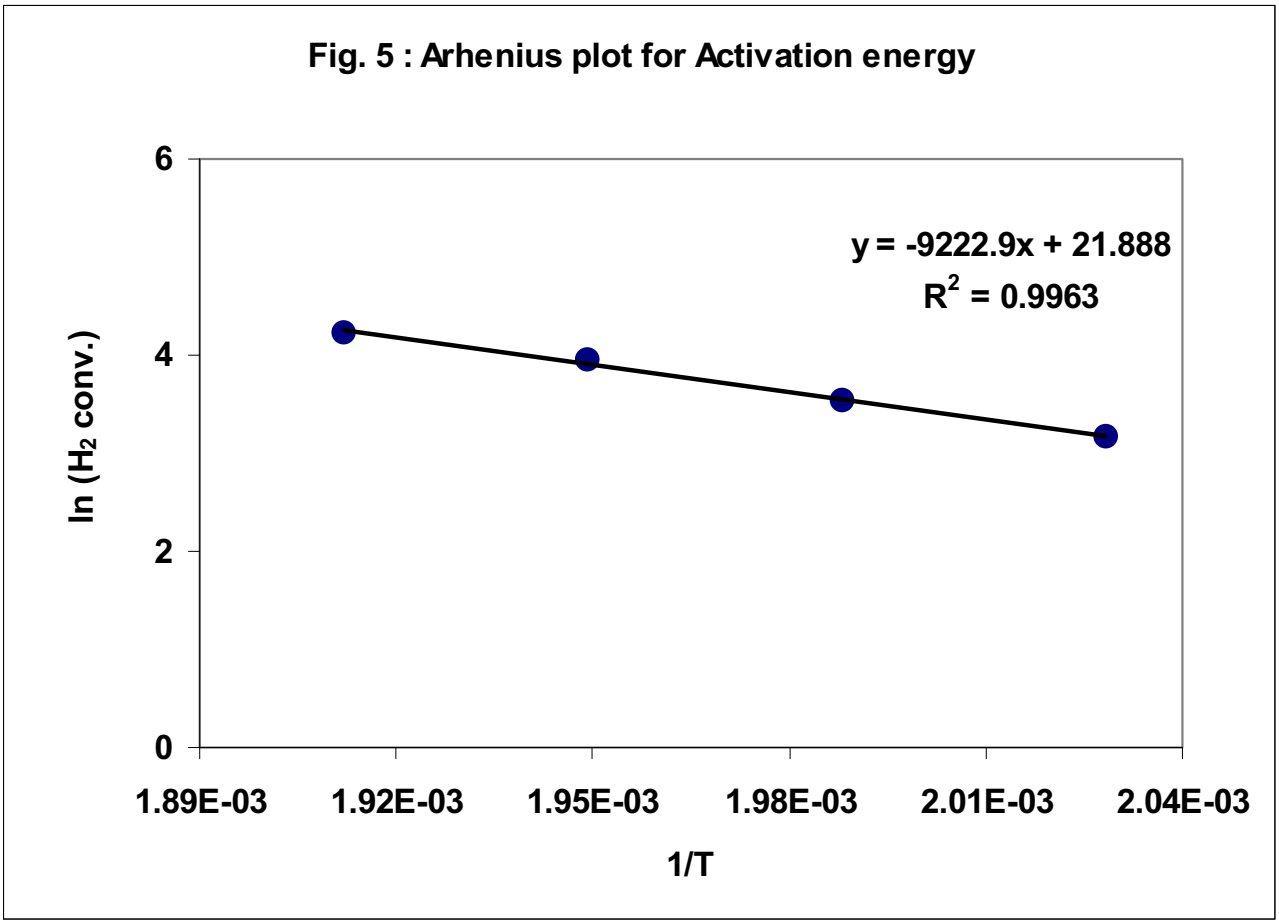
Fig. 5 : Arhenius plot for Activation energy
y = -9222.9x + 21.888
R2 = 0.9963
ln (H2 conv.)
6
4
2
0
1.89E-03
1.92E-03
1.95E-03
1.98E-03
2.01E-03
2.04E-03
1/T

Fig. 6 : Pressure effect on CO conversion over 0.2%Re-%Co $_2O_3$ at 230°C

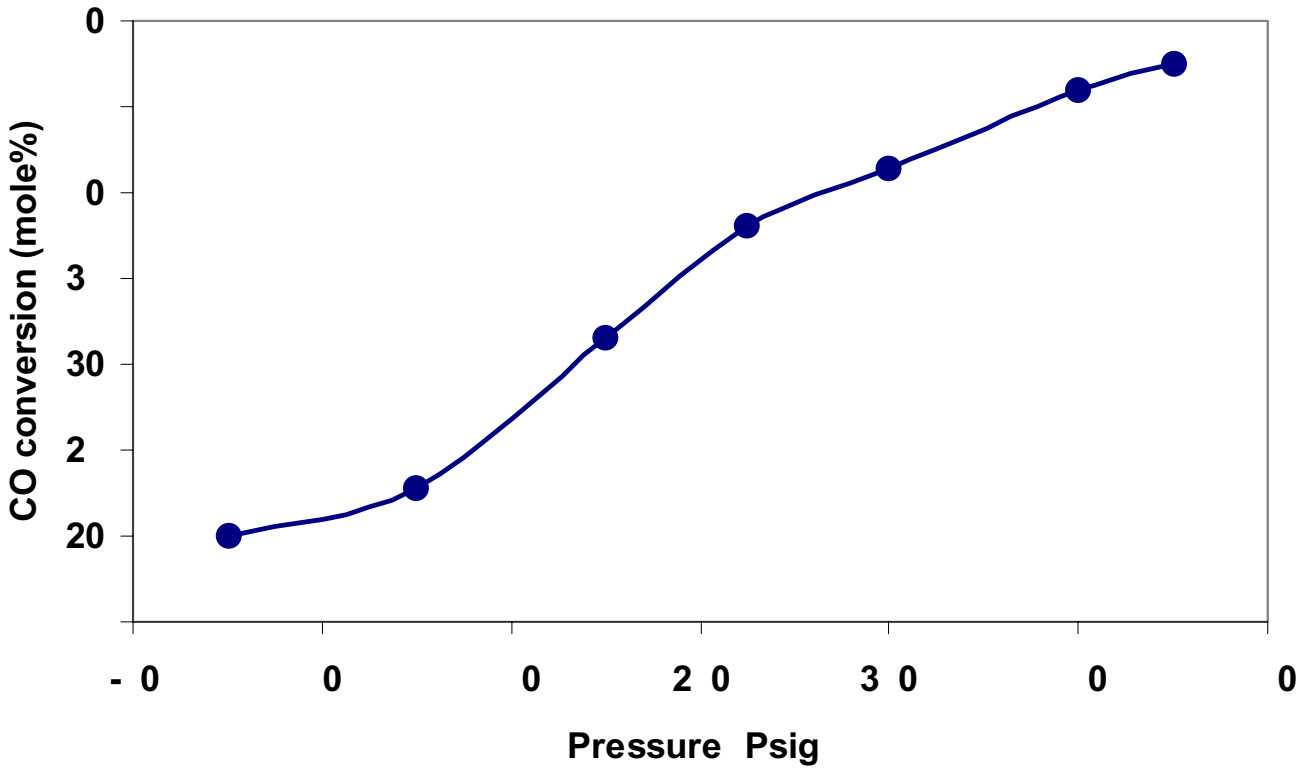

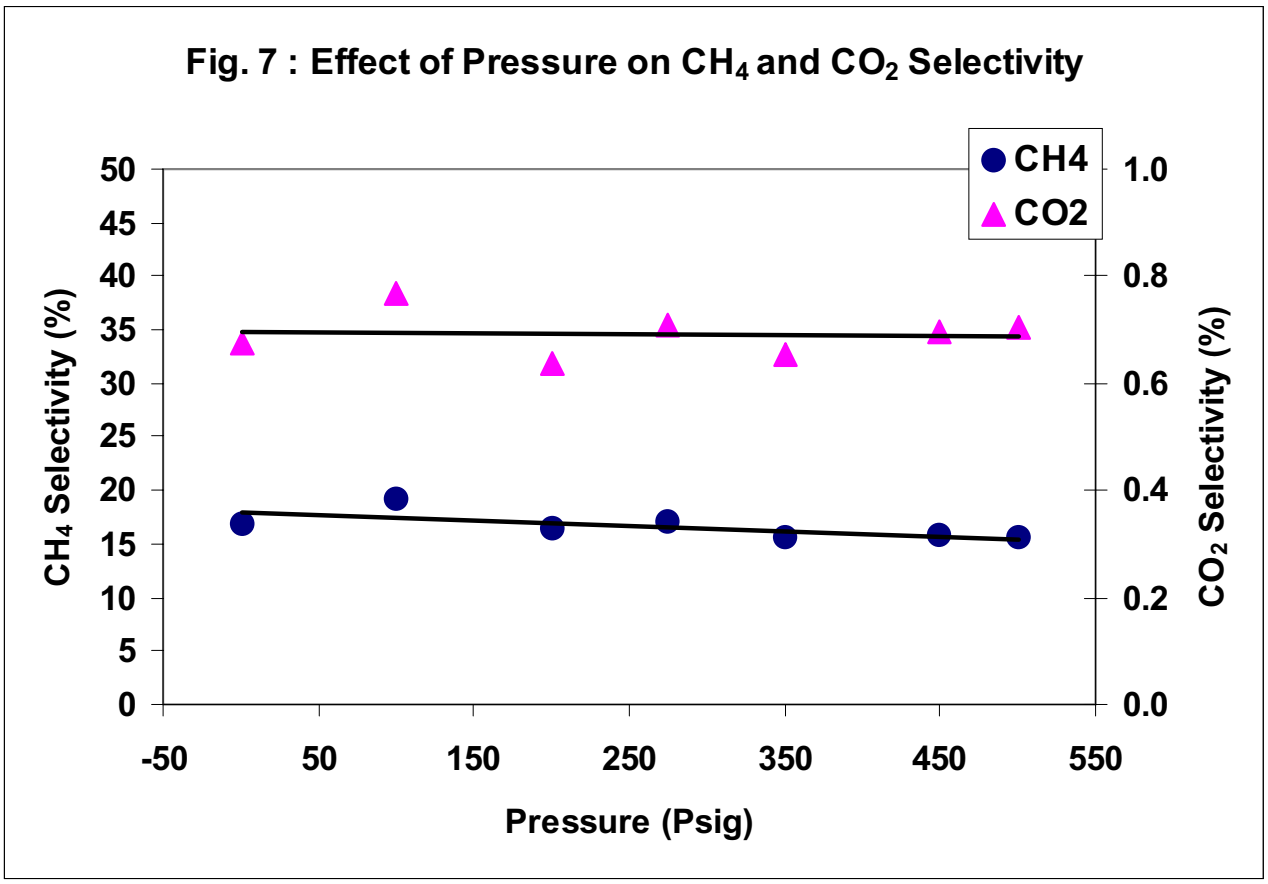
Fig. 7 : Effect of Pressure on CH_4 and CO_2 Selectivity
CH4
CO2
50
45
40
35
30
25
20
15
10
5
0
1.0
0.8
0.6
0.4
0.2
0.0
-50
50
150
250
350
450
550
CH_4 Selectivity (%)
CO_2 Selectivity (%)
Pressure (Psig)

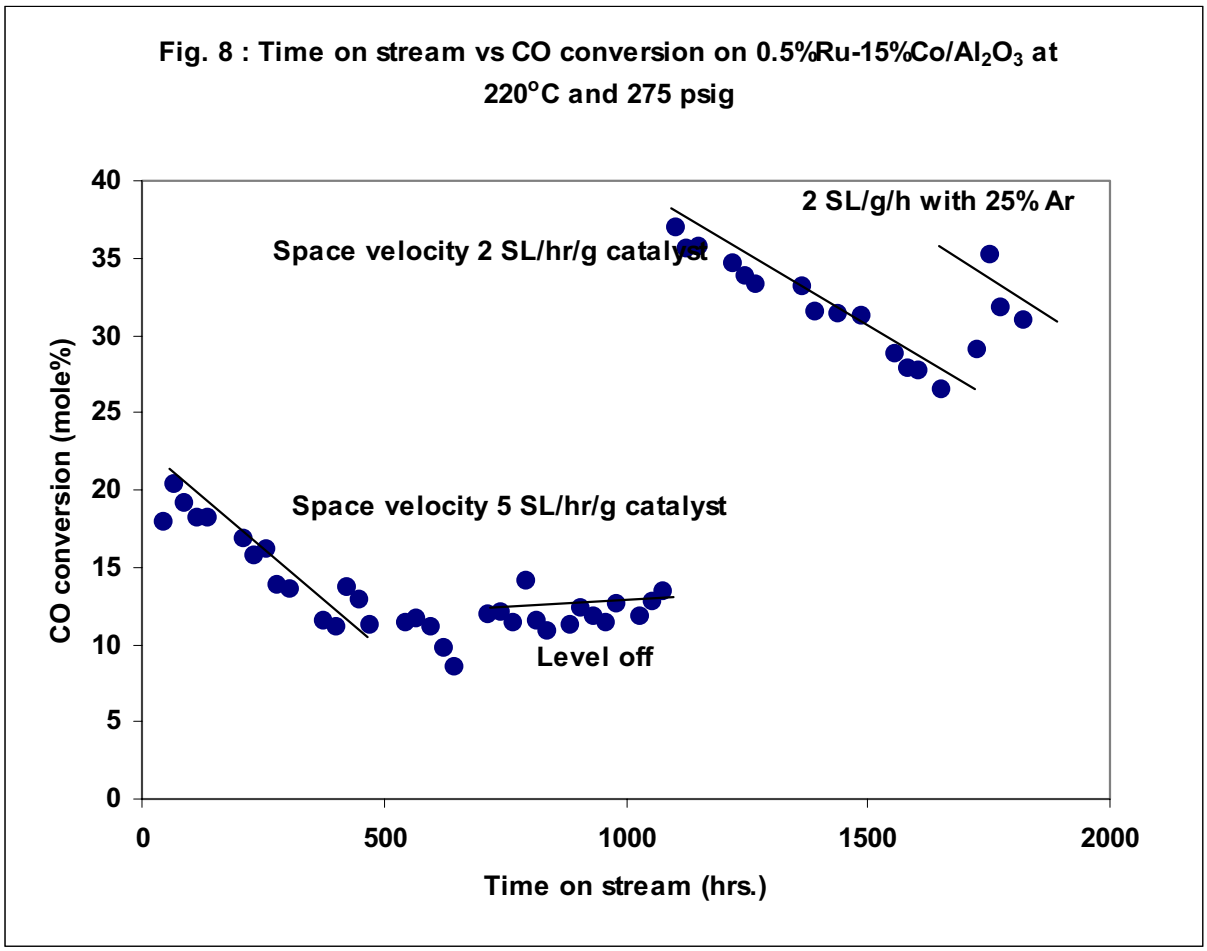
Fig. 8 : Time on stream vs CO conversion on 0.5%Ru-15%Co/Al2O3 at 220°C and 275 psig
2 SL/g/h with 25% Ar
Space velocity 2 SL/hr/g catalyst
Space velocity 5 SL/hr/g catalyst
Level off
CO conversion (mole%)
Time on stream (hrs.)
0
5
10
15
20
25
30
35
40
0
500
1000
1500
2000

Fig. 9 : Time on stream vs CO conversion over 0.5%Ru-20%Co/ZrO_2-SiO_2 at 220°C and 275 psig

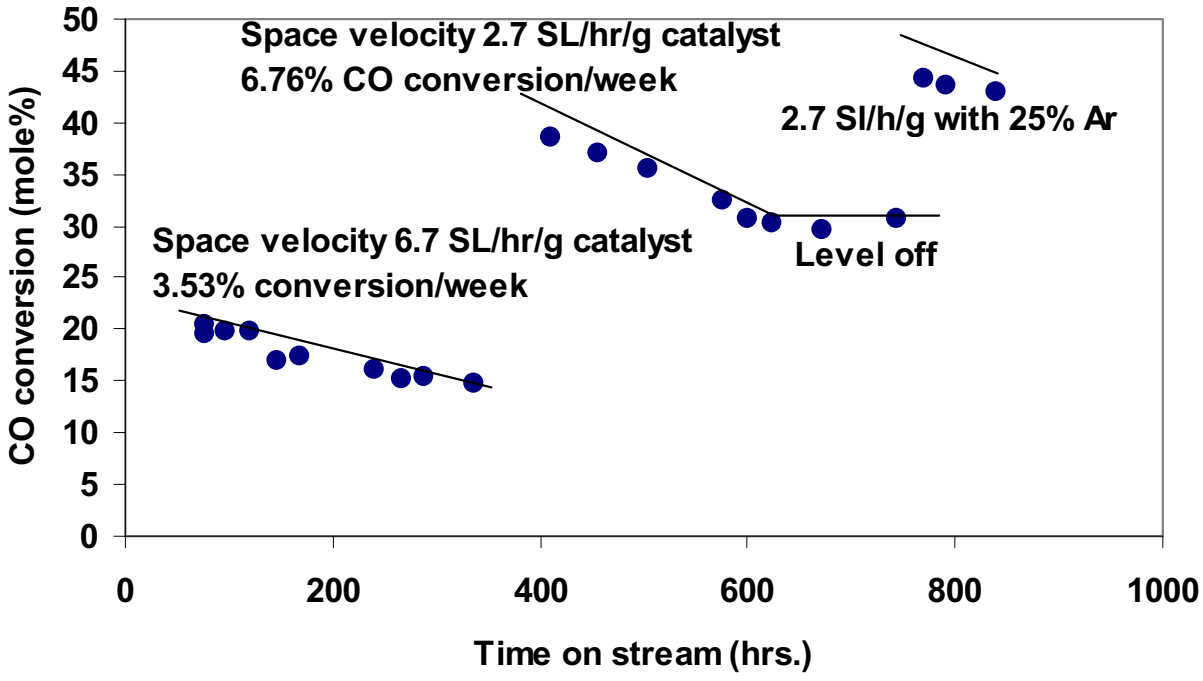

Fig. 10 : Time on stream vs CO conversion on 0.5%Pt-15%Co $_2O_3$ at 220°C and 275 psig

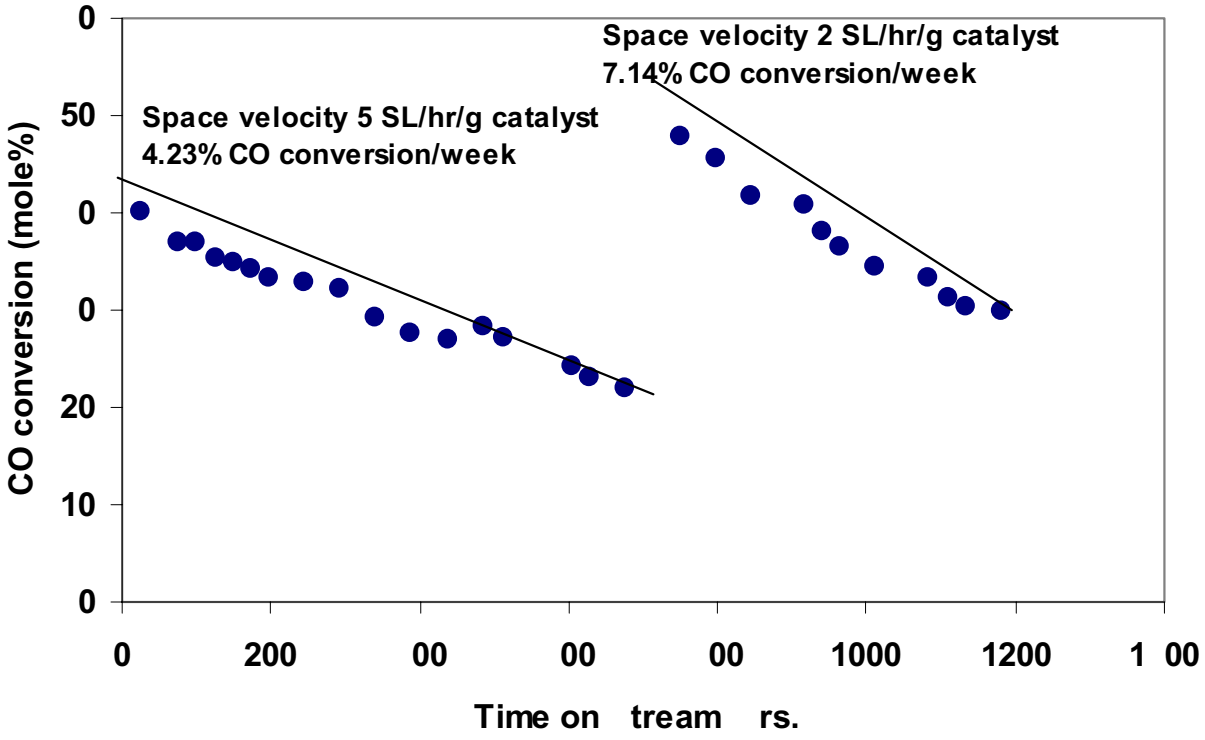

Fig. 11 : Time on stream vs CO conversion over 0.5% Pt-15% Co/Al_2O_3 at 210°C, 350 psig, H_2:CO = 2:1, GHSV = 5 SL/hr/g catalysts in Fixed-bed

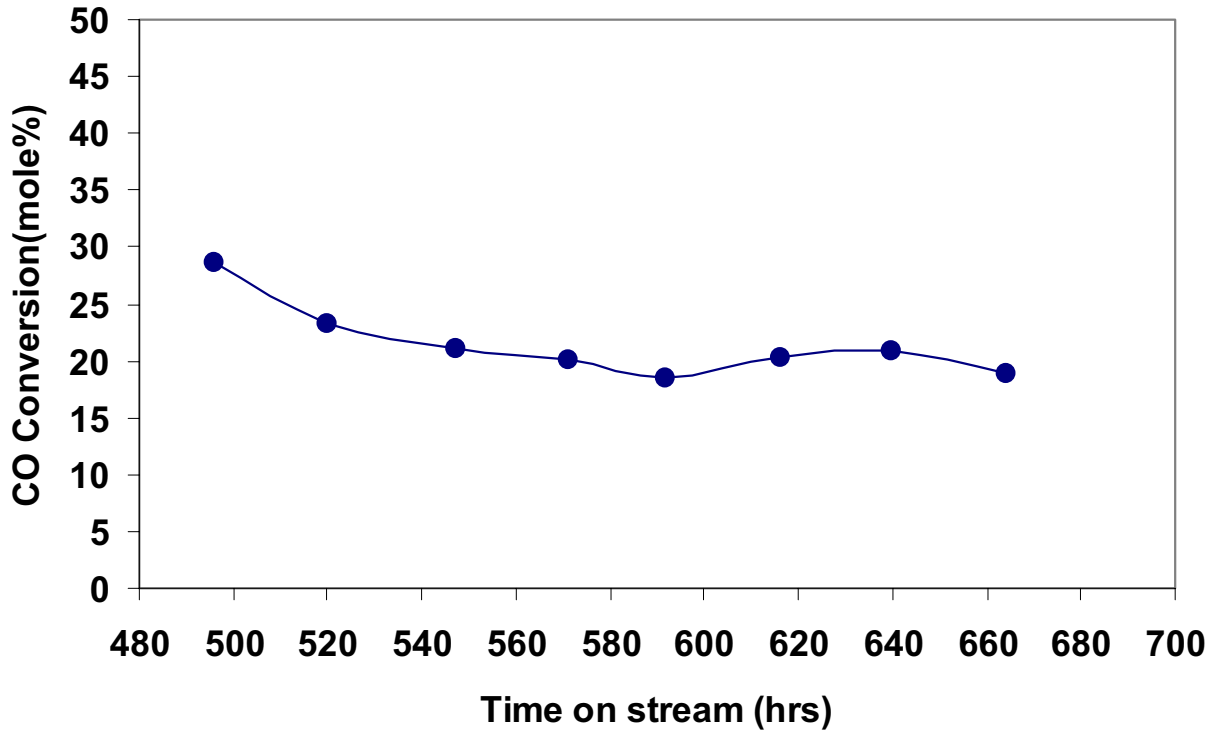

Task 10. Cobalt Catalyst Mechanism Study

The objective of this task is to determine the impact of secondary reactions on the relationship of cobalt Fischer-Tropsch catalysts under conditions appropriate to slurry bubble column reactors.

No scheduled activity to report.

Task 11. University of California, Berkeley (Subcontract)

The objective of this task is the characterization of the structure and function of active sites involved in the synthesis of high molecular weight hydrocarbons from CO and H_2 on multi-component catalysts based on Fe as the active component.

Table Of Contents

I. FISCHER-TROPSCH SYNTHESIS ON IRON CATALYSTS

1. Background

1.1. Structure and Function of Active Phases in Fischer-Tropsch Synthesis

Fe-based oxides have been used as commercial catalysts for Fischer-Tropsch synthesis (FTS) to produce a wide range of paraffin and olefin products, ranging from methane to high molecular weight waxes [1]. During activation in synthesis gas and subsequent FTS reaction, several phases including metallic iron, iron carbides and iron oxides can co-exist at steady-state conditions [2-5]. The relative amounts of these phases depend on various activation and reaction conditions, which also lead to different catalytic performance. Some researchers [6] have proposed that surface iron atoms are responsible for FTS activity, while others have considered surface carbides or a mixture of carbides [7,8] with metallic iron [9] to be the active phase. There are also some reports that suggest that magnetite Fe_3O_4 is the active FTS phase [10-12]. Although these studies have each provided some evidence to support its specific proposal about the active phase, the available information remains phenomenological and sometimes contradictory, and a direct method to identify the active phase during reaction and to count the number of active sites has remained elusive.

Based on our previous studies of the active phases and catalytic activity on Fe-Zn-K-Cu oxides [23], we have started in this reporting period the preparation of a new series of high surface area Fe-Zn catalysts and investigated the reduction and carburization process and catalytic activity in our search for alternate and superior catalysts for FTS reactions.

1.2. Effects of Zn, Ru (Cu) and K on Fe Oxides

Many components have been incorporated into Fe catalysts in order to improve their mechanical and catalytic properties. Our previous studies have shown that Zn, K and Cu [13-15] promote the catalytic properties of Fe oxides. Zinc oxide, as a non-reducible oxide at FTS conditions, appears to stabilize the surface area of Fe oxide precursors. Alkali, as a modifier of the adsorption enthalpies of H_2 and CO, has been reported to increase the selectivity to desired C_{5+} products. Copper promotes the carburization processes and decreases the temperature required for the activation of iron oxide precursors. According to our previous optimum composition of Fe-Zn-K-Cu (Zn/Fe=0.1, K/Fe=0.02, Cu/Fe=0.01), we have prepared a series of Zn and Fe co-precipitated oxides with constant Zn/Fe and K/Fe atomic ratios (Zn/Fe=0.1, K/Fe=0.02) and varying amounts of Ru (Ru/Fe=0-0.01). Ru is a very active FTS catalyst. Ru was chosen in order to improve the catalytic activity and to minimize unfavorable water gas shift reactions, which can be catalyzed by the Cu component on Fe catalysts. Also, K was added in order to increase wax and alkene yields, while decreasing the production of undesirable methane products. The same effects of K are expected on Fe-Zn-Ru-K catalysts. We have examined the surface area, bulk structure, required reduction and carburization temperatures, as well as the catalytic behavior of these catalysts, in order to identify optimum Ru contents that give maximum site densities and FTS reaction rates.

2. Synthesis Procedures

2.1 Higher Surface Area Fe-Zn-K-Cu Oxides

Fe-Zn-K-Cu catalysts were prepared by co-precipitation of iron and zinc nitrates following the procedure described in our previous report [18]. In order to produce high surface area samples, alcohol (isopropanol or ethanol) instead of water was used to wash the precipitates before drying the precipitates. Isopropanol or ethanol was employed to reduce the pore mouth pinching caused by the surface tension of intrapore liquids during drying processes. The subsequent impregnation procedure of an aqueous solution of potassium carbonate and copper nitrate using incipient wetness methods was the same as previously described [18].

2.2. Fe-Zn-Ru-K Oxides

All catalysts were prepared by co-precipitation of iron and zinc nitrates (Aldrich, 99+%) at a constant pH of 7.0 in order to form porous mixed oxides. Then, these oxide precursors were impregnated with a ruthenium (III) nitrosyl nitrate [$Ru(NO)(NO_3)_x(OH)_y$ (x+y=3)] (Aldrich, solution in dilute nitric acid, Ru 1.5%) and with an aqueous solution of potassium carbonate (Aldrich, 99+%) and copper nitrate (Aldrich, 99+%) using incipient wetness methods. The Zn/Fe oxide precursors were prepared first. Fe nitrate (1.4 M) and Zn nitrate (3.0 M) solutions were mixed at a given Zn/Fe atomic ratio (Zn/Fe=0.1). A solution of ammonium carbonate (Aldrich, 98%) (1 M) was prepared separately. Deionized water (~ 50 ml) was added into a large flask, which was heated on a hot plate with a magnetic stirrer and held at 353 K throughout the synthesis. The mixed Zn/Fe solution was added at 2 cm^3/min flow into the flask using a rotary pump. At the same time, the ammonium carbonate solution was fed separately, and its flow was controlled to maintain the slurry pH at 7±0.1, as monitored by a pH meter. The resulting precipitates (~20 g) were washed several times with about 1 *l* water per gram of catalyst, dried at 393 K overnight, and then treated in dry air at 623 K for 1 h. The air-treated powder was promoted with a ruthenium (III) nitrosyl nitrate solution [$Ru(NO)(NO_3)_x(OH)_y$ (x+y=3)] (Aldrich, solution in dilute nitric acid, Ru 1.5%) using incipient wetness protocols and then dried at 373 K. The dried material was treated in dry air at 623 K for 4 h. A similar process was used in order to promote samples with 2 at.% K using a K_2CO_3 solution (0.16 M). Finally, the dried material was treated again in dry air at 623 K for 4 h. These catalysts were pressed into pellets at 440 MPa, lightly crushed, and then sieved in order to retain the 80-140 mesh (100~180 μm) fraction used for FTS reactions and for all subsequent characterization studies.

3. Catalyst Characterization

3.1. Protocols for the Characterization of Fe-based FTS Catalysts

This research program addresses the synthesis and the structural and catalytic characterization of active sites in Fe-based catalysts for FTS. We have designed a matrix of samples consisting of a systematic range of multicomponent catalysts in order to

determine the number and type of surface sites present on fresh catalysts and on samples during and after FTS reaction (Table 1.1). Our objective is to develop rigorous relationships between the synthesis methods, the resulting catalyst structures, and their function in FTS reactions.

Table 1.1. Matrix of samples and characterization methods for FTS reaction

<table>
<tr><th colspan="3">Nominal Composition of the Catalysts</th><th rowspan="2">Characterization Before and After FTS</th><th rowspan="2">FTS reaction</th></tr>
<tr><th>Zn/Fe mole ratio</th><th>K/Fe (at.%)</th><th>Cu/Fe (at.%)</th></tr>
<tr><td rowspan="8">0</td><td rowspan="2">0</td><td>0</td><td rowspan="24">XRD

Surface area

In-situ XAS

H_2-TPR

CO-TPR</td><td rowspan="24">Effect of reaction condition

220 °C 21.4 atm

235 °C 21.4 atm

270 °C 5 atm

Effect of CO_2 addition

Isotopic studies</td></tr>
<tr><td>1</td></tr>
<tr><td rowspan="3">2</td><td>0</td></tr>
<tr><td>1</td></tr>
<tr><td>2</td></tr>
<tr><td>4</td><td>1</td></tr>
<tr><td rowspan="3">0.05</td><td>0</td><td>0</td></tr>
<tr><td>2</td><td>1</td></tr>
<tr><td>4</td><td>2</td></tr>
<tr><td rowspan="6">0.1*</td><td rowspan="2">0</td><td>0</td></tr>
<tr><td>1</td></tr>
<tr><td rowspan="3">2</td><td>0</td></tr>
<tr><td>1</td></tr>
<tr><td>2</td></tr>
<tr><td rowspan="2">4*</td><td>1</td></tr>
<tr><td>2*</td></tr>
<tr><td rowspan="3">0.2</td><td>0</td><td>0</td></tr>
<tr><td>2</td><td>1</td></tr>
<tr><td>4</td><td>2</td></tr>
<tr><td rowspan="6">0.4</td><td rowspan="2">0</td><td>0</td></tr>
<tr><td>1</td></tr>
<tr><td rowspan="3">2</td><td>0</td></tr>
<tr><td>1</td></tr>
<tr><td>2</td></tr>
<tr><td>6</td><td>1</td></tr>
<tr><th>Zn/Fe</th><th>Ru/Fe (at.%)</th><th>K/Fe (at.%)</th></tr>
<tr><td rowspan="4">0.1</td><td>0.5</td><td rowspan="2">0</td></tr>
<tr><td>1</td></tr>
<tr><td>0.5</td><td rowspan="2">2</td></tr>
<tr><td>1</td></tr>
</table>

* Samples treated by water and alcohol wash.

3.2. Crystal Structure

Figure 1 shows the X-ray diffraction patterns of the Fe-Zn oxide precursors prepared using different washing process and treated at different temperatures. At 534 K, Fe_2O_3 formed in water-washed Fe-Zn precursors as indicated by the sharp diffraction peaks matching those of standard patterns of Fe_2O_3. However, only broad Fe_2O_3-like diffraction peaks were detected on alcohol-washed Fe-Zn precursors, indicating that alcohol-washed Fe-Zn oxides consist of more finely dispersed Fe_2O_3. As the treatment temperatures increased to 623 K, the diffraction peaks become sharper on alcohol-washed Fe-Zn oxides, indicating the formation of larger crystallites of Fe_2O_3.

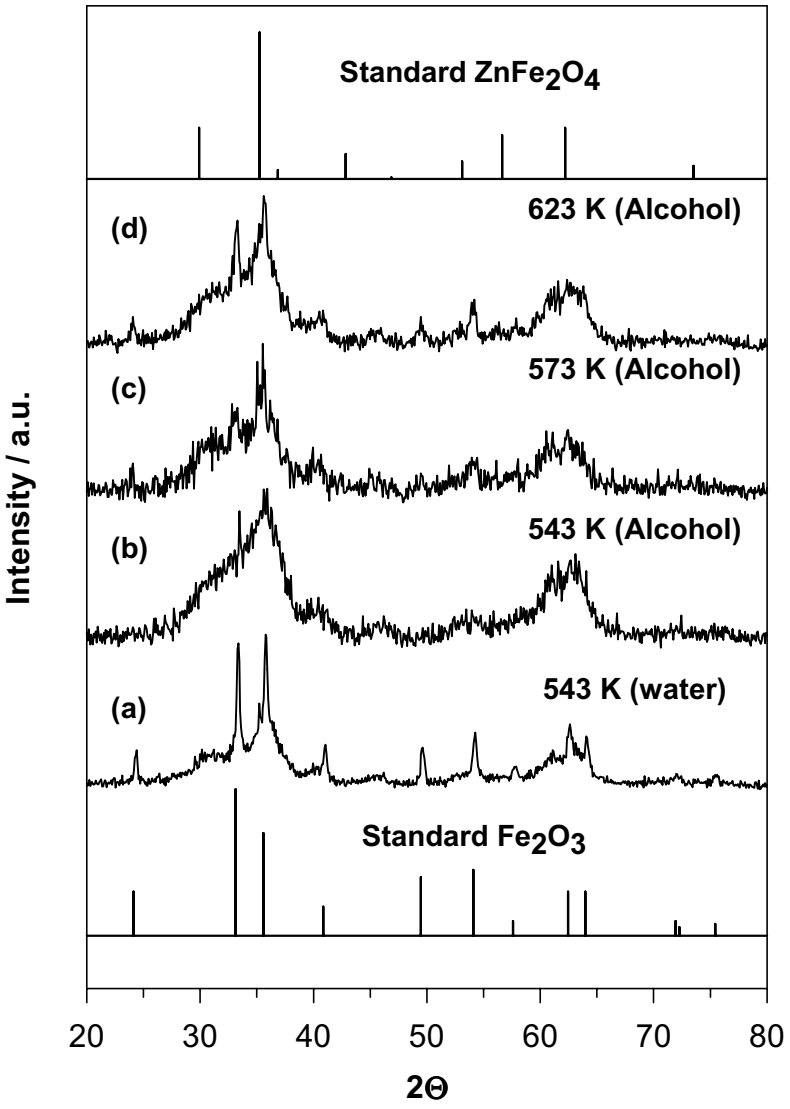

Figure 1. X-ray diffraction patterns of Fe-Zn oxide precursors. (a) water-washed precipitates, treated at 543 K for 4 h, (b) alcohol-washed precipitates, treated at 543 K for 4 h, (c) alcohol-washed precipitates, treated at 573 K for 4 h, (d) alcohol-washed precipitates, treated at 623 K for 4 h.

Figure 2 shows the X-ray diffraction patterns on Fe-Zn-K-Cu oxides after FTS reaction for 1 h. Fe_3O_4 was the only crystal phase detected on Fe-Zn, Fe-Zn-K2-Cu and Fe-Zn-K2-Cu1 oxide samples. No Fe carbides were detected on these samples. Since the conversion of Fe_3O_4 to Fe carbides is facile, it is expected that Fe carbides exist in an amorphous form on these samples, and that the compact Fe carbide layers covering over the Fe_3O_4 cores inhibit the carburization of Fe_3O_4. Substantial amount of χ-$Fe_{2.5}C$, despite poorly crystallized, was detected along with Fe_3O_4 crystallites on Fe-Zn-K4-Cu2 sample. This indicates that higher concentrations of K and Cu increase the extent of Fe_3O_4 carburization and also increases the formation rate of Fe carbide crystallites.

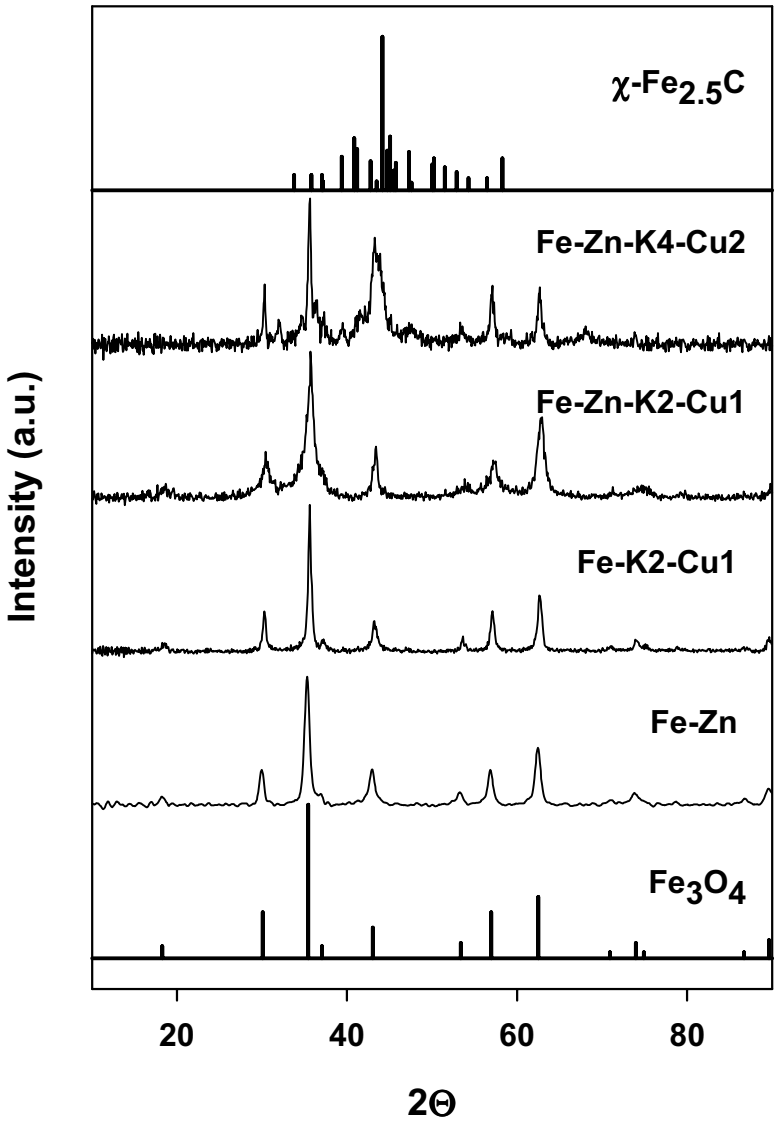

Figure 2. X-ray diffraction patterns of Fe-Zn-K-Cu oxides after FTS reaction at 250 ^oC for 1 h. (0.2 g sample, $H_2/CO=2$, flow rate 100 cm^3/min)

3.3. BET Surface Area

Many factors, including precipitate drying, treatment temperature and time, and the promoter impregnation, influence the surface area of the precursors. In this reporting period, these factors were systematically examined in order to increase the surface area of catalysts and to improve their catalytic performance.

3.3.1. Precipitate Drying Process and Treatment Temperature

Several approaches have been used to increase the surface area of the catalyst precursors. One attempt was the use of alcohol instead of waster to wash the precipitates in order to reduce the surface tension of the intrapore liquids during drying process. Ethanol or isopropanol was used, because they have much lower surface tension than water (20 vs. 60 nL/m). The precipitates were washed after precipitation with excess amount of alcohol in order to replace the water trapped in the intrapores of the precipitates.

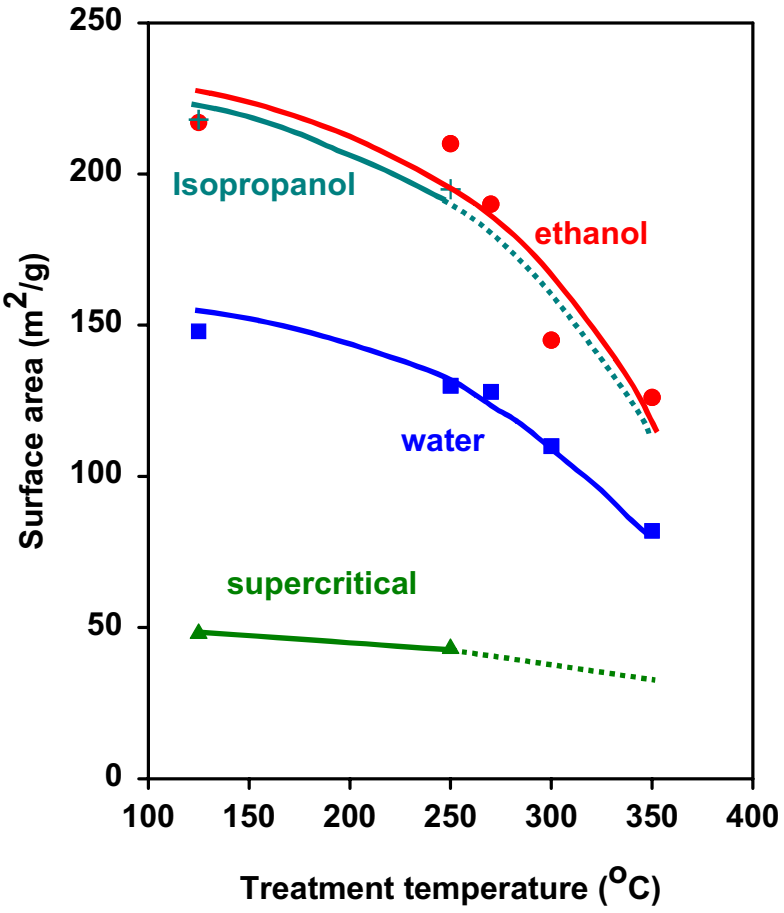

Figure 4. Surface area of Fe-Zn precipitates dried in different liquids and the surface area of the Fe-Zn precursors as a function of treatment temperature. Ethanol-washed (circle), isopropanol-washed (cross), water-washed (square), supercritical (triangle). (All the samples were treated at the give temperatures for 4 h).

Figure 4 shows the surface area of Fe-Zn precursors that pretreated in different liquids as a function of treatment temperature. Ethanol or isopropanol-washed precipitates showed higher Fe hydroxide surface areas than water-washed precipitates (215 vs 148 m^2/g). Alcohol fills the precipitate pores and prevents pore mouth pinching during drying by decreasing the surface tension of the intrapore liquids. The resemblance of the surface area for isopropanol-washed and ethanol-washed samples is consistent with their similar surface tensions. Isopropanol-containing precipitates treated at the critical conditions for isopropanol (235 ^oC, 48 atm) gave a surface area of only 48 m^2/g. Apparently H_2O from the decomposition of Fe hydroxides at these supercritical conditions led to sintering of the resulting Fe oxides. It appears that replacing water from the precipitates with low surface tension liquids during drying process is a key factor in increasing the surface area of the hydroxide and the subsequent oxide precursors.

After drying the precipitates at 125 ^oC for 12 h, the hydroxide powders were treated in dry air at different temperatures in order to examine the effect of treatment temperature on the surface area of the samples. The surface areas of resulting oxides decreased with increasing treatment temperature on both alcohol-washed and water-washed hydroxides, but the alcohol-washed hydroxides were more sensitive to the treatment temperatures. It appears that a treatment temperature of ~300 ^oC is suitable for decomposing hydroxide while not decreasing markedly the surface area of Fe oxides. Since water forms during hydroxide decomposition and it causes catalyst sintering, a high space velocity flow of dry air is required in order to minimize sintering during hydroxide decomposition (>2000 h^{-1}).

3.3.2. Promoter Impregnation

There are two different ways to impregnate promoters. One way is to impregnate promoters on Fe-Zn hydroxide precursors and then treat the sample at higher temperatures; the other way is to impregnate promoter on pretreated Fe-Zn oxide precursors. We are interested in learning whether the promoter impregnation or the sequence of impregnation influences the surface area of the samples. Figure 5 shows the surface areas of Fe-Zn hydroxides and oxides promoted with Ru and K as a function of treatment temperature. The addition of Ru to Fe-Zn hydroxide precursors decreased its surface area (220 vs 192 m^2g^{-1}), apparently because of the pore mouth pinching caused by the high surface tension of water during drying. Additional impregnation of K further decreased the surface area of Fe-Zn-Ru for the same reason. Each impregnation decreases the surface areas of the samples by ~10-20%.

These K and/or Ru-promoted Fe-Zn hydroxides were subsequently treated at different temperature in order to examine the effect of treatment temperature on their surface areas. Here, similar temperature effects were observed on promoted Fe-Zn oxides. The surface areas of K- and/or Ru-promoted Fe-Zn oxides decreased by ~50% by increasing the treatment temperature from 250 to 350 ^oC. Therefore, for the Fe-Zn based catalysts, the treatment temperature strongly influences their surface areas. Impregnating Ru onto Fe-Zn oxides, which were pretreated at 350 ^oC for 4 h, and subsequently treating the samples at 250, 300 and 350 ^oC respectively, showed almost identical surface area as that of the precursor Fe-Zn oxides. This indicates that once treated at higher temperatures, the

structure of Fe-Zn oxides is strong enough to prevent it from pore mouth pinching and further sintering. Also it implies that the length of treatment does not influence the surface areas of Fe-Zn oxides at given treatment temperatures.

Impregnation of promoters decreases the surface area of Fe-Zn oxide; the sequence of impregnation, however, appears not to influence the surface area of the resulting promoted Fe-Zn oxides at given treatment temperatures. It appears to be more efficient to impregnate promoters on Fe-Zn hydroxide precursors than on the Fe-Zn oxides obtained by thermal treatment of such precursors before impregnation.

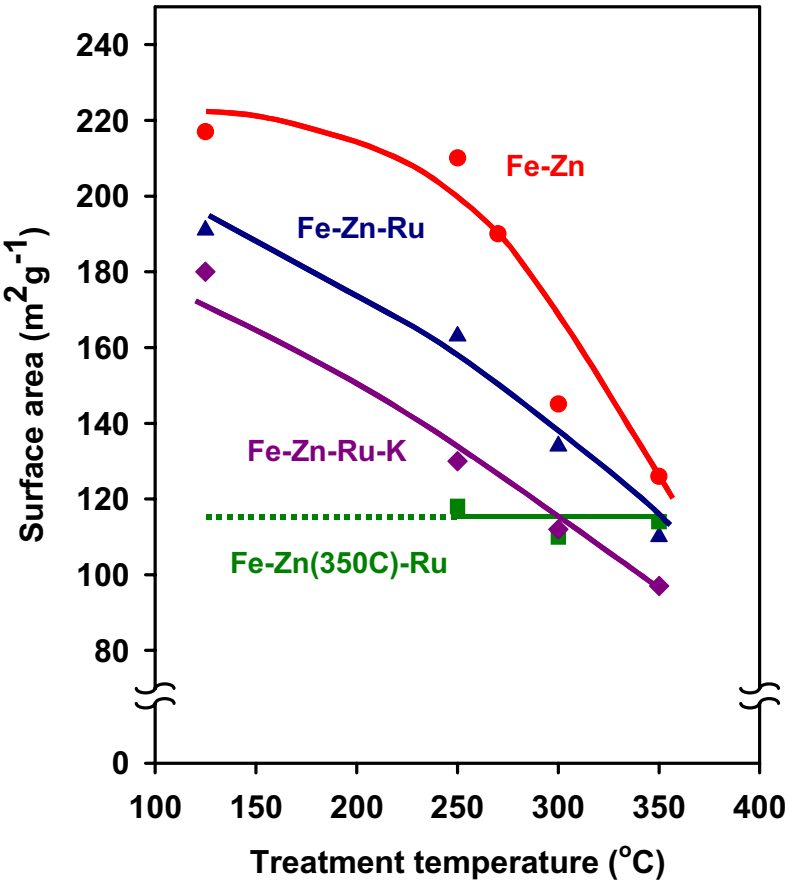

Figure 5. Surface area of Fe-Zn oxides promoted with Ru and K as a function of treatment temperature. (a) Fe-Zn oxide (circle), (b) Ru promoted on Fe-Zn hydroxide (triangle), (c) K and Ru promoted on Fe-Zn hydroxide (diamond), (d) Ru-promoted on Fe-Zn oxide pretreated at 350 °C for 4 h (square). (Zn/F=0.1, Ru/Fe=0.05, K/Fe=0.02, all samples were treated at given temperatures for 4 h)

3.4. Temperature-Programmed Reduction and Carburization of Fe-Zn-K-Cu Oxides

3.4.1. Reduction in H_2

Figure 6 shows the oxygen removal rate as a function of temperature for the reduction of Fe-Zn-K-Cu oxides in H_2. The reduction of K and Cu promoted Fe-Zn oxides started at

~100 K lower temperatures but finished at ~40 K higher temperatures than that on Fe-Zn oxide. This is apparently because Cu provides H_2 dissociation sites that decrease the reduction temperature, and K inhibits the reduction of Fe oxide in H_2 and thus prolongs their reduction processes. Fe-Zn-K2-Cu1 oxide started to reduce at almost identical temperatures but completed the reduction at ~40 K lower temperatures than the sample without Zn (Fe-K2-Cu1 oxide). Since K can titrate ZnO, especially at higher temperatures, the presence of Zn appears to weaken the inhibition effects of K on the reduction of Fe oxides. The Fe-Zn oxides promoted with higher concentrations of K and Cu (Fe-Zn-K4-Cu2) reduced at slightly higher temperatures than Fe-Zn-K2-Cu1. This suggests that the surface K/Cu ratio is probably slightly higher on Fe-Zn-K4-Cu2 than on Fe-Zn-K2-Cu1 sample.

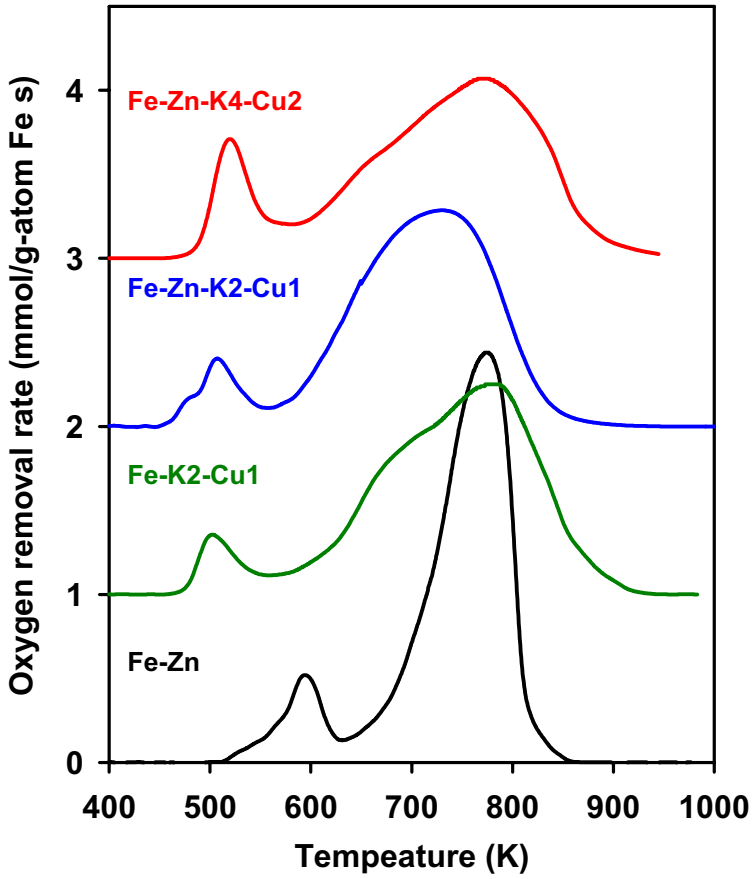

Figure 6. Oxygen removal rate as a function of temperature for the reduction of Fe-Zn-K-Cu oxides in H_2. (0.05 g sample, 10 ^{o}C/min ramping rate, 20 % H_2 in Ar, total flow rate 100 cm^3/min).

3.4.2. Reduction and Carburization in CO

Figure 7 shows oxygen removal and carbon introduction rates as a function of temperature during temperature-programmed reduction and carburization of Fe-Zn-K-Cu oxides in CO. K and Cu promoted Fe-Zn oxides reduced and carburized at ~30-50 K lower temperature than Fe-Zn oxides, apparently because K increases CO dissociation rates on Fe. The reduction and carburization profile of Fe-Zn-K4-Cu2 oxide in CO showed that the initial reduction/carburization temperature for Fe_3O_4 was lower and the carburization rates were slightly higher on Fe-Zn-K4-Cu2 than on Fe-Zn-K2-Cu1. These results again suggest that the surface K/Cu ratio probably is slightly higher on Fe-Zn-K4-Cu2 oxides than on the Fe-Zn-K2-Cu1 oxide. The increases in reduction and carburization rates on Fe-Zn-K4-Cu2 oxides imply its higher dispersion of Fe carbides, which in turn lead to higher reaction rates in FTS.

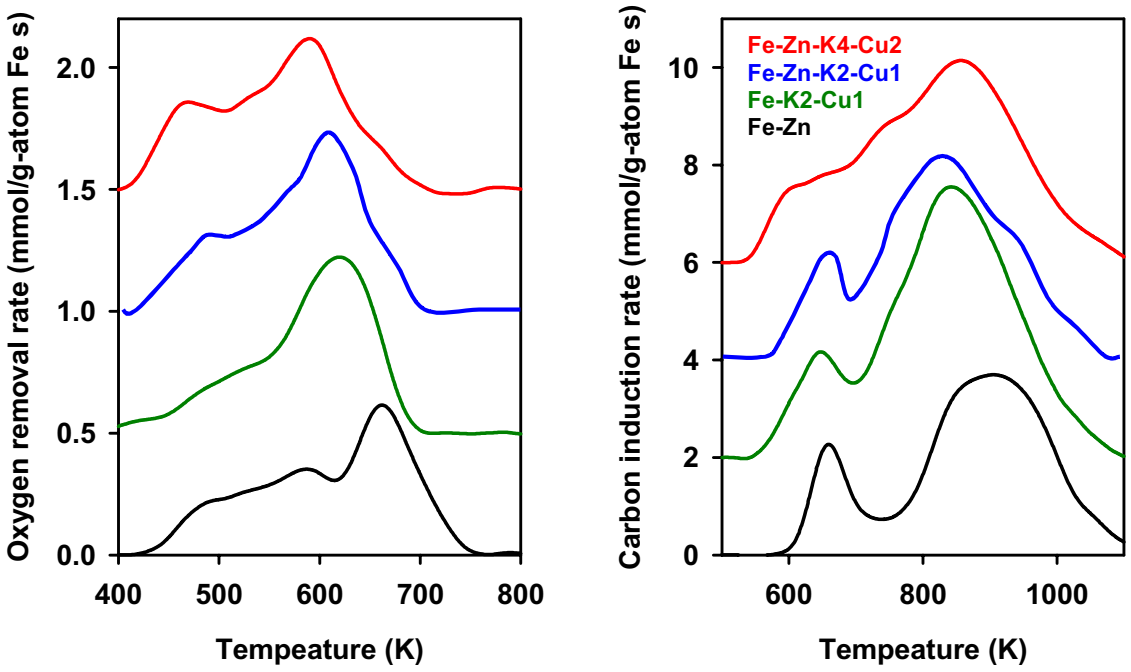

Figure 7. Oxygen removal and carbon introduction rates as a function of temperature during treatment of Fe-Zn-K-Cu oxides in CO. (0.05 g sample, 10 ^{o}C/min ramping rate, 20 % CO in Ar, total flow rate 100 cm^3/min)

3.5 CO chemisorption on Fe-Zn-K-Cu Oxides

Precipitated Fe oxides (0.2 g) were treated in flowing He (100 cm^3/min) at temperatures up to 573 K and then cooled down to 523 K. The He stream was switched to a flow of 60% synthesis gas (H_2/CO=2) in Ar (total flow rate 100 cm^3/min) at 523 K. After exposure to synthesis gas for 1 h, the synthesis gas stream was switched back to He and maintained at 523 K for an additional 1 h before cooling the sample to ambient temperature. The cooling process was accomplished by removing the furnace from the reactor and letting the reactor cool to ambient temperature. A flow of 20% CO in Ar

(total flow rate 100 cm^3/min) was passed through the samples for 0.5 h in order to carry out the adsorption. Physisorbed species were removed in flowing Ar (flow rate 100 cm^3/min) for 0.5 h at room temperature and the chemisorbed species evolved during temperature-programmed desorption (TPD) (10 K/min) and were measured using mass spectrometry.

In our previous quarterly report [22], our mass spectroscopy and X-ray absorption spectroscopy studies of the samples during the FTS reaction showed that these samples consist of bulk Fe_3O_4 and surface Fe carbides after FTS reaction at 523 K for 1 h. The He treatment at 523 K for 1 h removed most of the hydrocarbons formed during FTS reactions as no hydrocarbons were detected by the subsequent TPD in Ar. After CO chemisorption at ambient temperature and subsequent, H_2, CO and CO_2 were the only detectable desorption species. The amount of H_2O or CH_4 formed was negligible during temperature-programmed desorption in Ar, indicating that there is no interaction between adsorbed CO and hydrogen atoms during temperature-programmed desorption.

Table 3 Quantitative analysis of desorption species on Fe-Zn-K-Cu oxides during TPD in Ar at temperatures up to 820 K.

Desorbed species	Condi-tions	Amount desorbed (mmol/g-atom Fe)			
		Fe-Zn	Fe-K2-Cu1	Fe-Zn-K2-Cu1	Fe-Zn-K4-Cu2
H_2	(a)	12.4	48.3	51.1	74.4
	(b)	13.7	52.2	49.5	76.7
CO	(a)	3.0	33.6	40.2	47.3
	(b)	16.0	57.3	63.3	76.7
CO_2	(a)	1.4	23.3	25.0	27.9
	(b)	3.1	38.4	46.6	64.4
CO Chemisorption*		14.7	38.8	44.6	65.9

(a) TPD in Ar After FTS reaction at 523 K for 1 h.
(b) TPD in Ar after FTS reaction at 523 K for 1 h and CO chemisorption for 0.5 h at ambient temperature.
* CO chemisorption = $[(CO+CO_2)]_{(b)} - [(CO+CO_2)]_{(a)}$

All the samples were characterized by CO chemisorption in order to examine the effect of promoters on the CO adsorption behavior. Figures 8, 9 and 10 shows the H_2, CO and CO_2 desorption rates as a function of temperature after chemisorption of CO on Fe-Zn-K-Cu oxides after FTS reaction at 523 K for 1 h. Table 3 shows the quantitative analysis of the amounts desorbed H_2, CO and CO_2 during TPD in Ar up to temperatures of 820 K.

3.5.1. H_2 desorption

Figures 8a shows the H_2 desorption rates as a function of temperature after chemisorption of CO on the samples without adsorbing any titrants after FTS reaction at 523 K for 1 h. A broad H_2 desorption peak appeared at 500-800 K. This suggests that some hydrogen atoms (10-80 mmol H_2/g-atom Fe) remained strongly adsorbed on Fe carbide surfaces, and that they were not removed by flowing He at 523 K. The presence of promoters appeared not to influence the H_2 desorption temperatures but they significantly increased the amount of adsorbed H atoms. The presence of K and Cu increased the amount of absorbed H atoms four-fold over the sample without these promoters (51 mmol H_2/g-atom Fe on Fe-Zn-K2-Cu1 vs 12 mmol H_2/g-atom Fe on Fe-Zn), and higher concentrations of K and Cu gave even higher amount of absorbed H atoms. This reflects the fact that K and Cu increase the reduction and carburization rates on Fe oxides and produced higher surface area Fe carbides, which in turn provide more sites for H adsorption. Zn also slightly increased the density of adsorbed H species (51 mmol H_2/g-atom Fe on Fe-Zn-K2-Cu1 vs 48 mmol H_2/g-atom Fe on Fe-K2-Cu1). This is apparently because Zn as a structural promoter increases the surface area of Fe carbides despite the fact that Zn present as $ZnFe_2O_4$ also titrates part of Fe oxides. After adsorbing CO at ambient temperature for 0.5 h, the subsequent TPD shows that the H_2 desorption peak (Figure 8b) is unchanged, suggesting that these adsorbed H-atoms are not accessible by CO at ambient temperature.

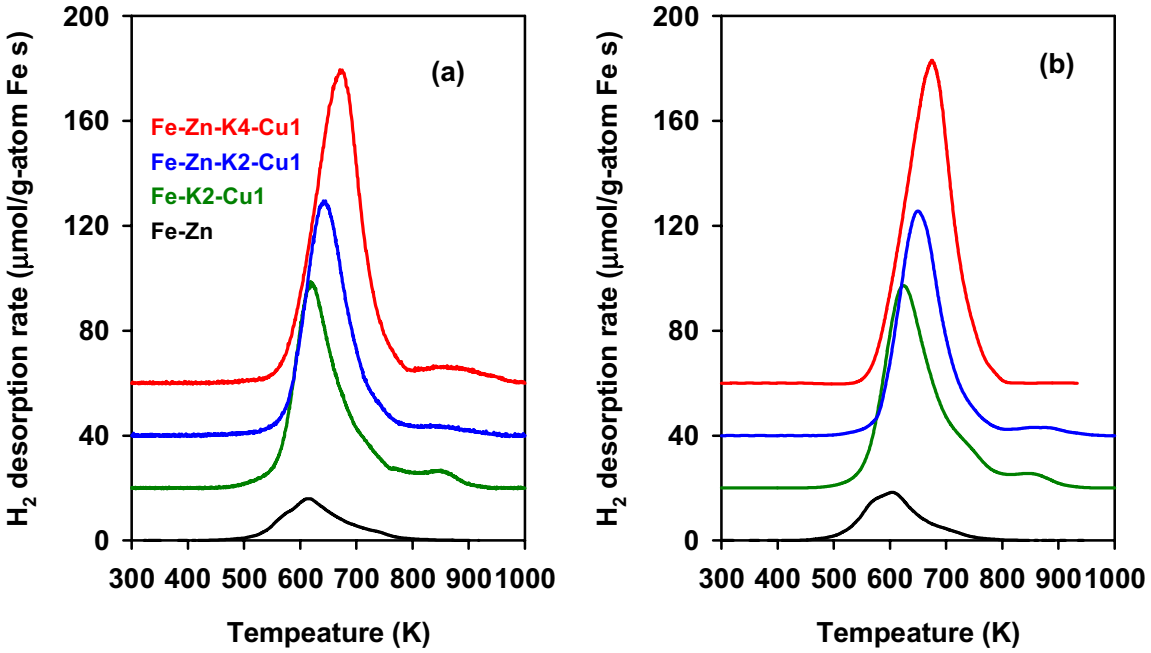

Figure 8. Temperature-programmed desorption of H_2 after FTS reaction and CO chemisorption. (0.2 g sample, K/Fe=0-0.04, Cu/Fe=0-0.02; FTS condition: 523 K, H_2/CO=2, total flow rate 100 cm^3/min; CO chemisorption: 20% CO in Ar, total flow rate 100 cm^3/min) (a): FTS at 523 K for 1 h, cooled in He, TPD in Ar; (b): FTS at 523 K for 1 h, cooled in He, CO chemisorption at room temperature for 0.5 h, TPD in Ar.

3.5.2 CO and CO_2 desorption

Figures 9 and 10 show the CO and CO_2 desorption rates as a function of temperature after chemisorption of CO on Fe-Zn-K-Cu oxides after FTS reaction at 523 K for 1 h. CO and CO_2 desorb simultaneously, implying that the desorption of CO is the rate-determining step. When CO desorbs, it may react readily with distant adsorbed O species, forming CO_2. Figures 9a and 10a show the desorption peaks of CO and CO_2 immediately after FTS reaction and before chemisorption. The asymmetric CO and CO_2 desorption peaks show that they consist of a small amount of weakly adsorbed C species, which can be attributed to the molecular desorption at 550-700 K, and a large amount of strongly adsorbed C species, which resulted from a recombination process of C and O at 700-800 K. The desorption peaks at temperatures higher than 800 K can be ascribed to the surface graphite deposits left behind by the Boudouard reaction. The presence of promoters resulted in greater CO or CO_2 desorption uptakes than the samples without them but they did not influence the desorption temperature. This suggests that the presence of K or Cu increases the density but not the type of the adsorption sites for FTS. Figures 9b and 10b show the desorption of CO and CO_2 after CO chemisorption. Compared with Figure 9a and Figure 10a, the amount of desorbed CO and CO_2 are both higher after CO chemisorbed than before CO chemisorption. The difference between these two curves is the amount of CO chemisorbed on the Fe carbides, which also reflects the total amount of accessible adsorption sites on Fe carbides.

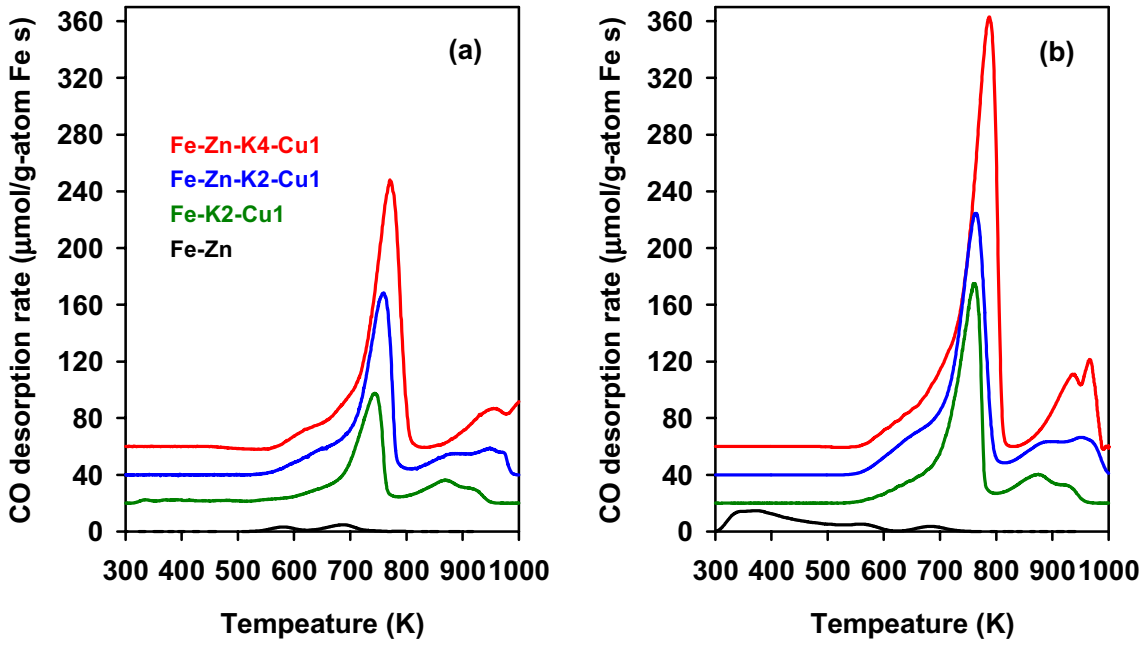

Figure 9. Temperature-programmed desorption of CO_2 after FTS reaction and CO chemisorption. (0.2 g sample, K/Fe=0-0.04, Cu/Fe=0-0.02; FTS condition: 523 K, H_2/CO=2, total flow rate 100 cm^3/min; CO chemisorption: 20% CO in Ar, total flow rate 100 cm^3/min) (a): FTS at 523 K for 1 h, cooled in He, TPD in Ar; (b): FTS at 523 K for 1 h, cooled in He, CO chemisorption at room temperature for 0.5 h, TPD in Ar.

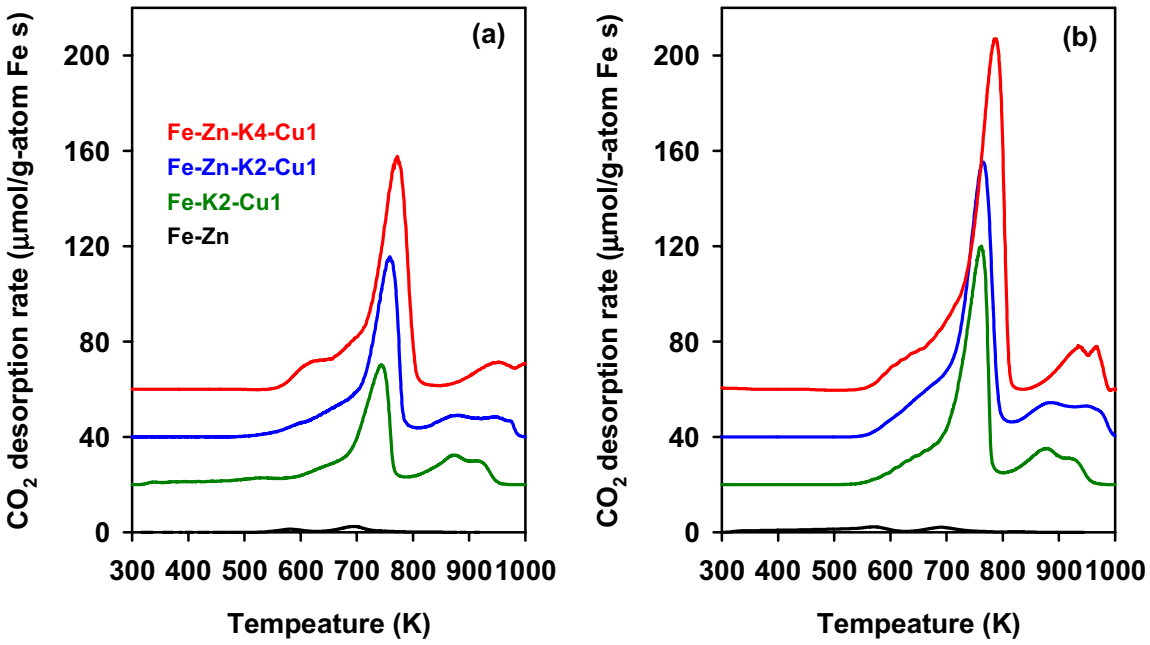

Figure 10. Temperature-programmed desorption of CO_2 after FTS reaction and CO chemisorption. (0.2 g sample, K/Fe=0-0.04, Cu/Fe=0-0.02; FTS condition: 523 K, H_2/CO=2, total flow rate 100 cm^3/min; CO chemisorption: 20% CO in Ar, total flow rate 100 cm^3/min) (a): FTS at 523 K for 1 h, cooled in He, TPD in Ar; (b): FTS at 523 K for 1 h, cooled in He, CO chemisorption at room temperature for 0.5 h, TPD in Ar.

As shown in Table 3, K and Cu promoted Fe-Zn oxides show much larger amounts of adsorbed CO than Fe-Zn oxides (44.6 vs. 14.7 mmol C/g-atom Fe), indicating that the presence of K and Cu increase the density of adsorption sites for FTS reaction. Higher concentrations of K and Cu on Fe-Zn-K4-Cu2 sample led to even higher density of CO chemisorption sites (65.9 mmol C/g-atom Fe). Comparing the amount of CO chemisorbed on Fe-K2-Cu1 (38.8 mmol C/g-atom Fe) with that on Fe-Zn-K2-Cu1 (44.6 mmol C/g-atom Fe), the amount of CO chemisorbed is slightly higher on the Zn-containing sample, reflecting the structural promotion effect of ZnO. It appears that the presence of K, Cu, or Zn increases the extent of reduction and carburization of Fe oxide, leading to higher surface area of Fe carbides, which consequently provides more sites for CO chemisorption and for FTS reactions.

3.5.3. Surface Area of Fe-Zn-K-Cu Oxides after FTS Reaction

Surface area measurements were performed on Fe-Zn-K-Cu oxides after FTS reaction but immediately before CO chemisorption studies in order to establish a correlation between the surface area of the catalysts and the adsorption site densities. The surface areas of all samples decreased significantly after exposure to synthesis gas at 523 K for 1 h, suggesting the shrinkage of Fe oxide particles after carbide formation. The higher surface area oxide precursors (50-120 m^2/g) tend to have higher surface areas after FTS reaction for 1 h (20-40 m^2/g). The amount of CO adsorbed correlates well with the

surface area of the catalysts on K and Cu promoted samples. In contrast, the amount of CO adsorbed is relatively low on Fe-Zn sample, but the surface area is relatively high compared with K and Cu containing samples. This is probably because Zn titrates some of the Fe oxides despite its structural promotion effect on increasing the surface area of Fe oxides. The relatively high surface area may not all be available for CO chemisorption and FTS reactions.

Table 4. Surface areas (m^2g^{-1}) of Fe-Zn-K-Cu (Zn/Fe=0.1) samples after FTS in synthesis gas up to 250 ^oC for 1 h

Sample	Fe-Zn	Fe-K2-Cu1	Fe-Zn-K2-Cu1	Fe-Zn-K4-Cu2
Before FTS	115	52	65	120
FTS 1 h	39	23	30	42

In conclusion, CO chemisorption can be used as a useful measure of the site density of catalysts. The amount of CO chemisorbed on the catalysts is in good agreement with their surface areas. The presence of K and Cu significantly increases the reduction and carburization rates on Fe oxides, leading to higher surface area Fe carbides, which in turn provide more sites for CO chemisorption and FTS reactions. Zn also increases the site density on Fe oxides, but it does not increase the number of sites in proportion to its increase in surface because of its apparent ability to block some Fe-derived active sites.

4. FISCHER-TROPSCH SYNTHESIS ON IRON CATALYSTS

4.1. FTS reactions on a high surface area Fe-Zn-Cu-K catalyst

During this reporting period, FTS reactions were carried out on a high surface area Fe-Zn-Cu-K sample (Zn/Fe=0.1, Cu/M=0.02, K/M=0.04), the synthesis procedure of which has been described in Section 2 (surface area for the precarburized samples being 120 m^2/g compared to 65 m^2/g earlier). The aim was to compare the behavior of the two samples for the FTS reaction and to determine the effects of surface area on FTS performance.

The activity and selectivity on the high surface area Fe-Zn-Cu-K sample is compared in this section with that of the low surface area Fe-Zn-Cu-K sample (Zn/Fe=0.1, Cu/M=0.02, K/M=0.04) reported earlier [18-20]. The CO conversion on the two catalysts is shown as a function of reciprocal space velocity in Figures 11; the CO consumption rate is shown as a function of the CO conversion in Figure 12. The CO conversion and CO rates are significantly higher on the high surface area catalyst than on the low surface area sample indicating an increase in the number of active sites available for the FTS reaction.

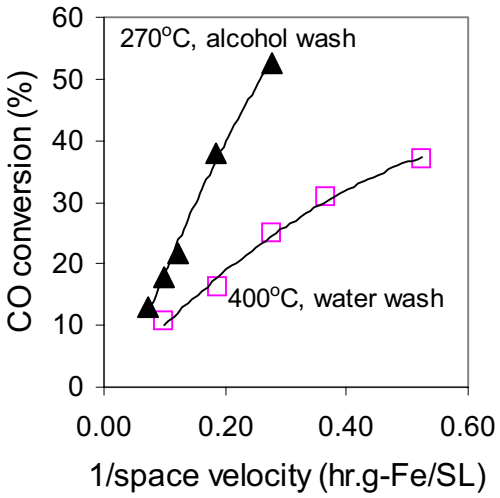

Figure 11. CO conversion as a function of reciprocal CO space velocity on the Fe-Zn-Cu-K catalyst samples (Calcined at 400°C, water wash; and Calcined at 270°C, alcohol wash), 220°C, 31.6 atm, $H_2/CO=2$.

A summary of the FTS data obtained on the two samples is presented in Table 4. The hydrocarbon productivity is approximately 2.3 times higher on the high surface area sample, consistent with the two-fold increase in surface area. Hence the increase in activity is likely to an increase in the number of available sites rather than a change in the activity per site (Figure 13). CO_2 selectivities are almost identical in the two cases. The higher surface area sample has a slightly higher selectivity to light hydrocarbons and a lower C_{5+} selectivity. It is possible that the concentration of Cu and K atoms per Fe is

smaller on the high surface area sample than the low surface area sample and this may account for the observed small decrease in product molecular weight and in olefin content as exemplified by the difference in the *1*-hexene/*1*-hexane ratio.

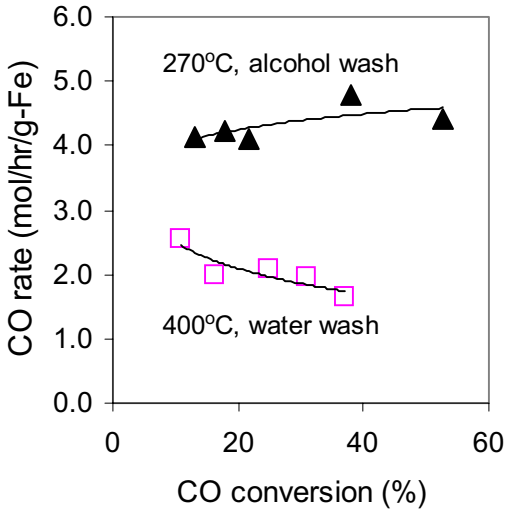

Figure 12. CO rate as a function of CO conversion on the Fe-Zn-Cu-K catalyst samples (Calcined at 400°C, water wash; and Calcined at 270°C, alcohol wash), 220°C, 31.6 atm, H_2/CO=2.

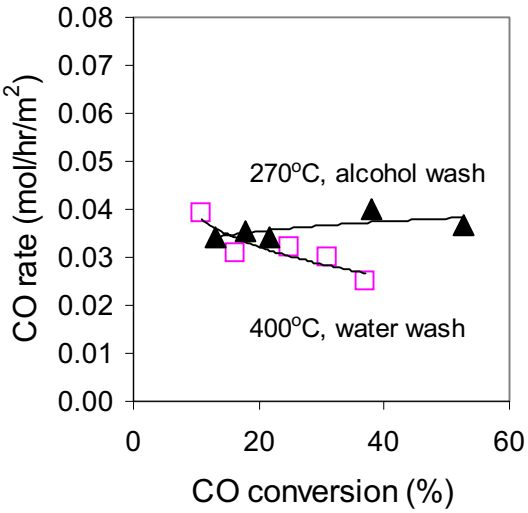

Figure 13. CO rate per surface area as a function of CO conversion on the Fe-Zn-Cu-K catalyst samples (Calcined at 400°C, water wash; and Calcined at 270°C, alcohol wash), 220°C, 31.6 atm, H_2/CO=2.

Table 4. Comparison of FTS parameters on the two Fe-Zn-Cu-K samples at 220°C, 31.6 atm, H_2/CO=2.

	FeZnCu1K2 (low SA)	FeZnCu2K4 (high SA)
CO conversion (%)	37	38
HC productivity (g/hr.g-Fe)	388	856
CO_2 selectivity (%)	21.8	22.4
HC selectivity (CO_2-free)		
CH_4 selectivity (%)	1.9	2.6
C_2-C_4 (%)	10.8	13.9
C_{5+} (%)	87.3	83.5
1 -C_6H_{12}/*1* -C_6H_{14}	2.2	2

From our results, it is clear that the effect of surface area on the catalysts is an improvement in the dispersion of the Fe_xC crystallites, which results in an increased activity for the FTS reaction. However, the chemical environment on the catalyst appears to be unchanged as explained by similar product selectivities.

4.2 Effect of H_2/CO ratio on the FTS rate and selectivity on a Fe-Zn-Cu-K catalyst

During the current reporting period, the behavior of a Fe-Zn-Cu-K catalyst (Zn/Fe=0.1, Cu/M=0.02, K/M=0.04) with high H_2/CO ratios was studied at 200°C, the temperature used for FTS reactions on Co-based catalysts. The aim of this study was to test if the Fe catalyst behaves similar to the Co/SiO_2 catalyst (studied previously) under similar surface H*/CO* ratios [20-23]. Since the hydrogen surface coverage is much higher on Co than on Fe, the experiments were conducted with a H_2/CO ratio that is much higher than 2. The catalyst was first pretreated in synthesis gas while the temperature was ramped from 25°C to 150°C at 10°C/min and from 150 to 270°C at 1°C/min. The temperature was held constant at 270°C for 1 hour and then the reactor was cooled to 200°C and the pressure was set at the desired values. Our preliminary approach involved the matching of the CH_4 selectivities on both catalysts at 200°C. This comparison was performed at low CO space times in order to exclude the significant contributions from autocatalytic water effects on Co catalysts. The CH_4 selectivities were similar when the experiments were conducted at a H_2/CO ratio of 20 on the Fe-Zn-Cu-K catalyst.

The CO conversion on the Co and Fe catalysts (H_2/CO=2 and 20) are shown in Figure 14 as a function of the reciprocal CO space velocity. The FTS run on the Fe catalyst at low H_2/CO ratio showed the lowest CO conversions. Upon increase in the H_2/CO ratio, the CO conversion increases at identical space velocities indicating a positive dependence of the FTS reaction rate on the hydrogen partial pressure. Similarly, the CO rate is shown in Figure 15 as a function of the CO conversion at both conditions. The Co/SiO_2 catalyst had a much higher CO conversion and rate than the Fe catalyst at this temperature.

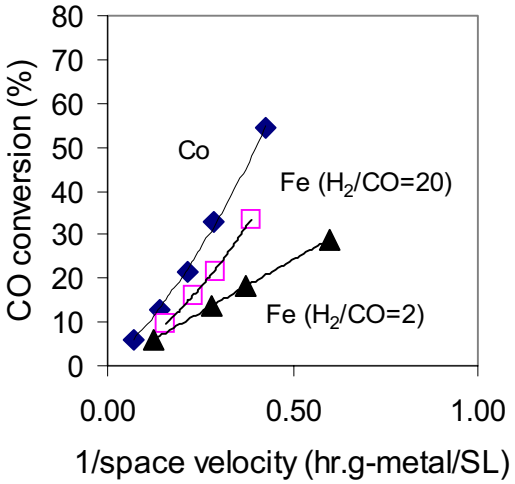

Figure 14. CO conversion as a function of reciprocal CO space velocity at 200°C on Co/SiO_2 (H_2/CO=2, 20 atm), Fe-Zn-Cu-K (H_2/CO=2, 20 atm) and Fe-Zn-Cu-K (H_2/CO=20, 32 atm).

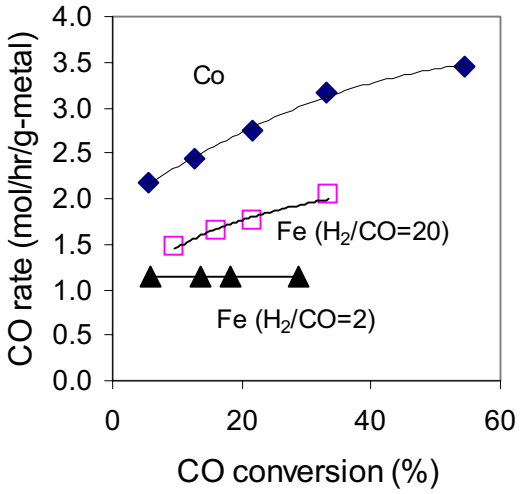

Figure 15. CO consumption rate as a function of CO conversion at 200°C on Co/SiO_2 (H_2/CO=2, 20 atm), Fe-Zn-Cu-K (H_2/CO=2, 20 atm) and Fe-Zn-Cu-K (H_2/CO=20, 32 atm).

The CO_2 selectivity in all three cases is shown as a function of CO conversion in Figure 16. While the Fe catalyst operated at a H_2/CO ratio of 2 showed higher CO_2 selectivities and exhibited a linear increase in its selectivity as a function of the CO conversion, a different behavior is observed when the same catalyst is operated at higher H_2/CO ratios (20). At these conditions, the CO surface coverage is much smaller than in the case of the former and hence the predominant mode of oxygen removal is as H_2O instead of CO_2. Since the slope of the CO_2 selectivity curve at the high H_2/CO ratio is almost zero, the secondary water gas shift reaction does not appear to take place at these conditions and the only route of CO_2 formation is *via* oxygen removal using CO.

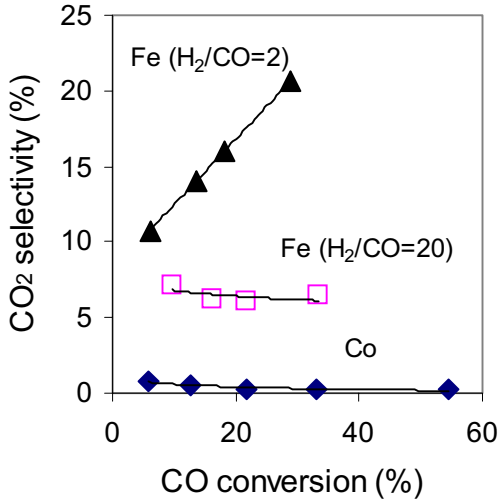

Figure 16. CO_2 selectivity as a function of CO conversion at 200°C on Co/SiO_2 (H_2/CO=2, 20 atm), Fe-Zn-Cu-K (H_2/CO=2, 20 atm) and Fe-Zn-Cu-K (H_2/CO=20, 32 atm).

The CH_4 selectivity curve of the Fe-Zn-Cu-K catalyst at $H_2/CO=20$ almost matches that of Co/SiO_2, and significantly higher than that of the Fe-Zn-Cu-K at $H_2/CO=2$ (Figure 17). The higher hydrogen surface concentration in the case of Fe-Zn-Cu-K leads to a significantly lower C_{5+} selectivity compared to the other two cases (Figure 18).

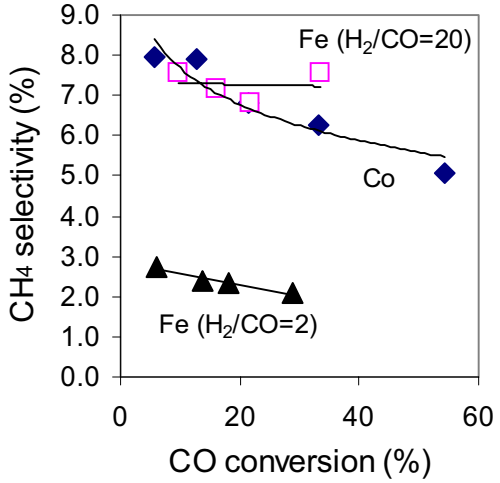

Figure 17. CH_4 selectivity as a function of CO conversion at 200°C on Co/SiO_2 ($H_2/CO=2$, 20 atm), Fe-Zn-Cu-K ($H_2/CO=2$, 20 atm) and Fe-Zn-Cu-K ($H_2/CO=20$, 32 atm).

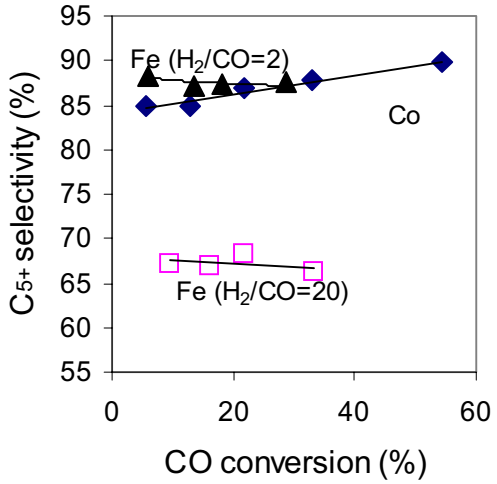

Figure 18. C_{5+} selectivity as a function of CO conversion at 200°C on Co/SiO_2 ($H_2/CO=2$, 20 atm), Fe-Zn-Cu-K ($H_2/CO=2$, 20 atm) and Fe-Zn-Cu-K ($H_2/CO=20$, 32 atm).

The α-olefin/*n*-paraffin ratio is shown as a function of the carbon number in Figure 19. At high surface hydrogen coverages, the Fe-Zn-Cu-K catalyst has a much lower olefin content than at the H_2/CO ratio of 2. For carbon numbers beyond C_2, the olefin/paraffin ratio is also lower than on the Co/SiO_2 catalyst. The *1*-hexene/*n*-hexane ratio is plotted as

a function of reciprocal space velocity in Figure 20. The decrease in this ratio on the Co/SiO_2 with space time has previously been attributed primarily to readsorption of olefins followed by subsequent chain growth and termination as higher carbon number chains [25,26]. The *1*-hexene/*n*-hexane ratio on the Fe catalyst, on the other hand, is independent of space time in both cases. This indicates the absence of any secondary hydrogenation or readsorption on these Fe catalysts.

A closer look at the C_5 selectivity distribution on the Fe-Zn-Cu-K catalyst at $H_2/CO=20$ shown in Figure 21, confirms the conclusions drawn above. While the total C_5 content is unchanged, the *1*-pentene and *n*-pentane contents are also relatively unchanged with space time pointing to the absence of secondary reactions. At such high surface hydrogen coverages on the Fe catalyst, chains get terminated at low carbon numbers with high probabilities, which explains the lower C_{5+} selectivity than at $H_2/CO=2$. While the methane selectivities in the case of the Fe catalyst ($H_2/CO=20$) and Co are similar, hydrocarbon selectivities from C_2 and beyond are lower for the Co catalyst because of a combination of the following two effects: a decreased intrinsic probability of termination of hydrocarbon chains at low carbon numbers and the readsorption of low and intermediate molecular weight olefins and their contribution to further chain growth [25,26].

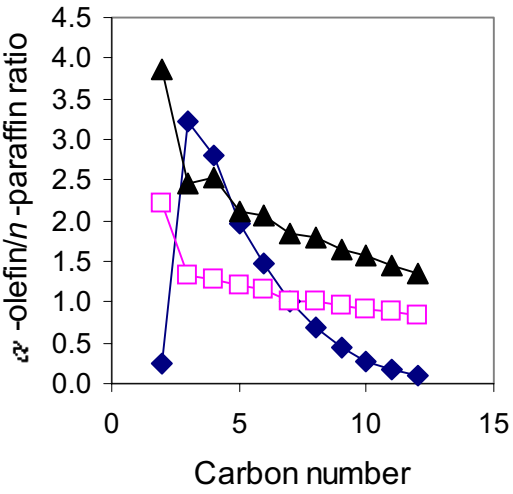

Figure 19. α–Olefin/*n*-paraffin ratio as a function of carbon number at 200°C on Co/SiO_2 (200°C, $H_2/CO=2$, 20 atm), Fe-Zn-Cu-K ($H_2/CO=2$, 20 atm) and Fe-Zn-Cu-K ($H_2/CO=20$, 32 atm).

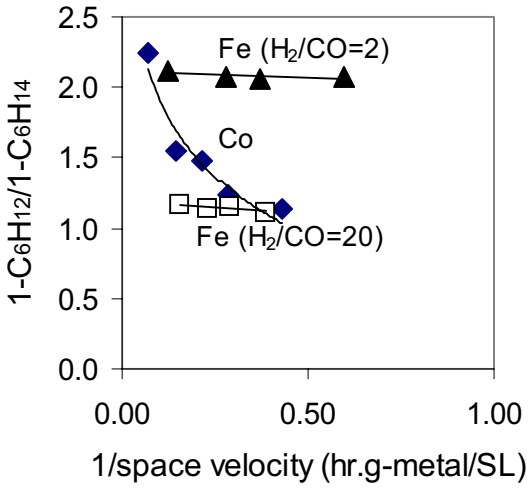

Figure 20. *1*–C_6H_{12}/*n*-C_6H_{14} ratio as a function of reciprocal space velocity at 200°C on Co/SiO_2 (200°C, $H_2/CO=2$, 20 atm), Fe-Zn-Cu-K ($H_2/CO=2$, 20 atm) and Fe-Zn-Cu-K ($H_2/CO=20$, 32 atm).

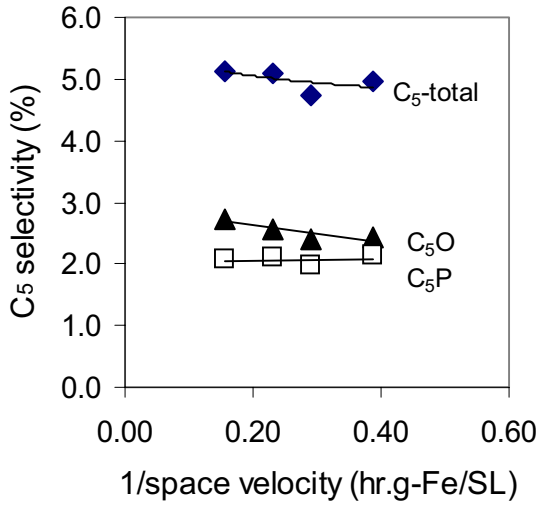

Figure 21. C_5 selectivity distribution as a function of CO conversion at 200°C on Fe-Zn-Cu-K (H_2/CO=20, 32 atm).

Further analysis of the wax samples collected during the above runs is expected to completed in the next quarter and this is expected to provide more information on the chain growth mechanism on the catalysts.

4.3. FTS reactions on Ru-promoted Fe-Zn-K catalysts: Effect of Ru loading

During the previous quarter, studies were continued with Fe-Zn-Ru-K catalysts in order to confirm the promotion effects of Ru for the FTS reaction [24]. The effect of Ru loading (0 to 1 at.%) on the activity and selectivity behavior of a Fe-Zn-K catalyst was studied.

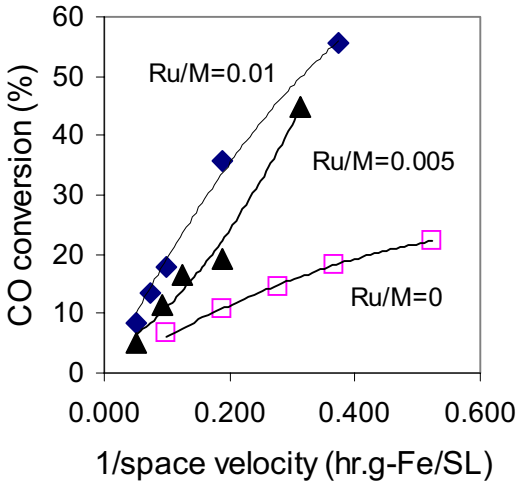

Figure 22. CO conversion as a function of reciprocal space velocity on the catalysts. Fe-Zn-Ru1-K (Zn/Fe=0.1, K/M=0.02, Ru/M=0.01), Fe-Zn-Ru0.5-K (Zn/Fe=0.1, K/M=0.02, Ru/M=0.005), Fe-Zn-K (Zn/Fe=0.1, K/M=0.02, Ru/M=0); 220°C, 31.6 atm, H_2/CO=2.

As shown in Figure 22, the CO conversion increases upon addition of Ru to Fe-Zn-K. Ru-addition was attempted initially to overcome one of the deficiencies of the Cu-promoted Fe-Zn-K catalysts, which is its high CO_2 selectivity. However, our results show that the replacement of Cu by Ru do not lead to a decrease in CO_2 selectivity during the FTS reaction. In fact, an increase in the Ru concentration in the 0-1 at.% range also increased CO_2 selectivities (Figure 23). Ru appears to increase CO_2 formation *via* its primary mode.

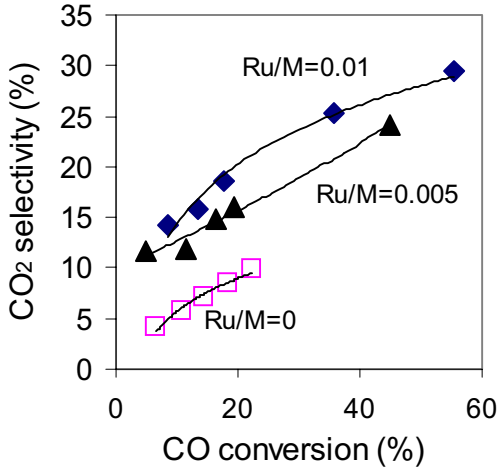

Figure 23. CO_2 selectivity as a function of CO conversion, Fe-Zn-Ru1-K (Zn/Fe=0.1, K/M=0.02, Ru/M=0.01), Fe-Zn-Ru0.5-K (Zn/Fe=0.1, K/M=0.02, Ru/M=0.005), Fe-Zn-K (Zn/Fe=0.1, K/M=0.02, Ru/M=0); 220°C, 31.6 atm, H_2/CO=2.

Table 5. FTS reaction parameters for Ru- promoted catalysts at 220°C, 31.6 atm, H_2/CO=2

	Fe-Zn-K	Fe-Zn-Ru-0.5-K	Fe-Zn-Ru1.0-K
CO conversion (%)	18.3	19.4	17.8
CO rate (mol/hr.g-at. Fe)	1.3	2.4	4.2
HC productivity (g/hr/kg.Fe)	290	514	860
CO_2 selectivity (%)	8.5	15.9	18.6
HC selectivities (CO_2 free)			
CH_4 (%)	1.8	2.2	2.6
C_2-C_4 (%)	10.7	11.4	11.9
C_{5+} (%)	87.5	86.4	85.5
1 -C_6H_{12}/*1* -C_6H_{14}	2.0	1.7	1.8

The addition of Ru also leads to a small decrease in the product molecular weight (lower C_{5+} selectivity) and to a small increase in the paraffin content due to the ability of Ru to improve hydrogen dissociation on the surface. However, since these selectivity effects are negligible compared to the extent of promotion of the FTS rates, the primary role of Ru is in improving the dispersion of Fe_xC sites on the catalyst surface. It is also possible that Ru prevents sintering of the catalyst during the pretreatment step.

Even though the addition of Ru leads to much higher hydrocarbon productivities than on Cu-promoted catalysts, the high cost of Ru makes the Ru contents used in this study impractical for commercial use [27-30]. However, Ru-promoted catalysts are attractive because they could be activated at much lower temperatures than the Cu-promoted ones.

II FISCHER-TROPSCH SYNTHESIS ON COBALT CATALYSTS

1. Study of the effect of H_2/CO ratios on a 21.9% Co/SiO_2 catalyst

During the previous quarter, the behavior of a Co/SiO_2 catalyst was studied at conditions involving lower H_2/CO ratios and higher temperatures typical of Fe-based FTS reactions. The aim of this study was to test if the Co catalyst behaves similar to Fe when the surface H*/CO* ratio approach each other. The experiments were carried out with a 21.9% Co/SiO_2 catalyst at 220°C and at a H_2/CO ratio of 1.0. Prior to the reaction, the catalyst sample was pretreated in H_2 (200 ml/g/min) from 25°C to 325°C at the rate of 10°C/min followed by reduction at 325°C for 1 h. The reactor was then cooled down to 160°C in H_2, the flow of synthesis gas (H_2/CO=2) was started, and the pressure was set to 20 atm and finally the temperature raised to 200°C. Upon verification of a data point at this condition, the CO pressure was raised to obtain a H_2/CO ratio of 1.0 (P_{H2}=19.6 atm, the same as that used for Fe-based catalysts at 220°C). Finally the temperature of the reactor was gradually increased to 220°C in order to prevent any initial exotherms or hot spots.

Fig. 24 shows CO conversion as a function of reciprocal space velocity for the Fe-Zn-Cu-K (high surface area) catalyst and a 21.9% Co/SiO_2 catalyst with H_2/CO=1 at 220°C. At this temperature, the Co catalyst has a higher CO conversion and rate than the Fe-Zn-Cu-K sample. Since it is likely that the CO rate has a negative dependence on the CO conversion, and the CO gas phase concentration is lower in the case of Co, this result indicates that the Co/SiO_2 has a significantly higher activity than the Fe-based sample. It is also interesting to note that the CO conversion rate increases with increase in time which points out to the existence of the autocatalytic water effect even under these conditions on Co [19-22].

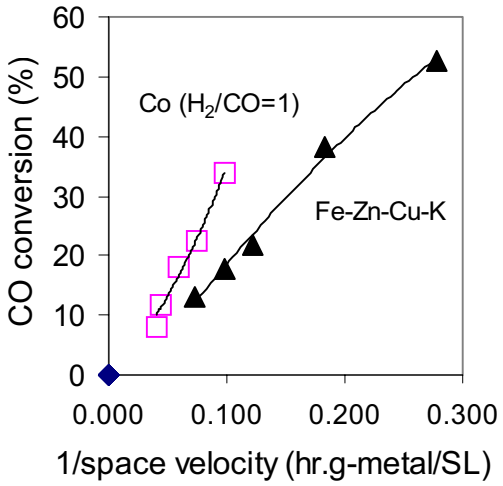

Figure 24. CO conversion as a function of reciprocal space velocity at 220°C on Co/SiO_2 (H_2/CO=1, 43.6 atm), and Fe-Zn-Cu-K (H_2/CO=2, 31.6 atm).

At this temperature, the Co/SiO_2 catalyst is likely to have a high selectivity to methane at $H_2/CO=2$. With a lower H_2/CO ratio, the CH_4 selectivity is significantly smaller (Figure 25) and decreases with increasing space time due to the fact that water plays a role in promoting chain growth as observed previously [19,25,26]. Similarly the C_{5+} selectivity increases with increasing space time on the Co/SiO_2 sample (Figure 26). While the CH_4 selectivity of the Co/SiO_2 sample ($H_2/CO=1$) is significantly smaller on Fe-Zn-Cu-K ($H_2/CO=2$), the C_{5+} selectivities are almost identical at low space times. This is because olefins (C_2 and beyond) undergo readsorption on the Co catalyst and terminate at higher carbon numbers with a high probability unlike in the case of the Fe catalyst on which such a mechanism does not take place.

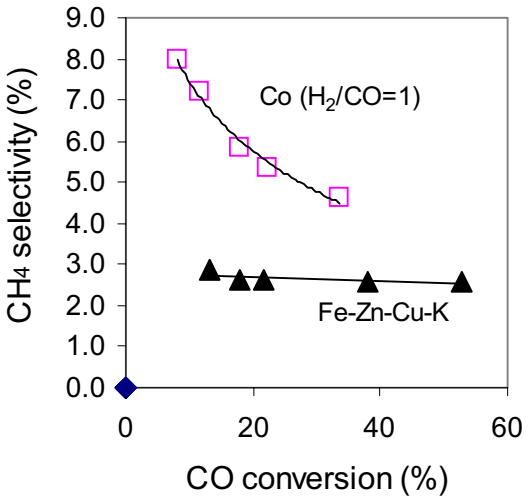

Figure 25. CH_4 selectivity as a function of CO conversion at 220°C on Co/SiO_2 ($H_2/CO=1$, 43.6 atm), and Fe-Zn-Cu-K ($H_2/CO=2$, 31.6 atm).

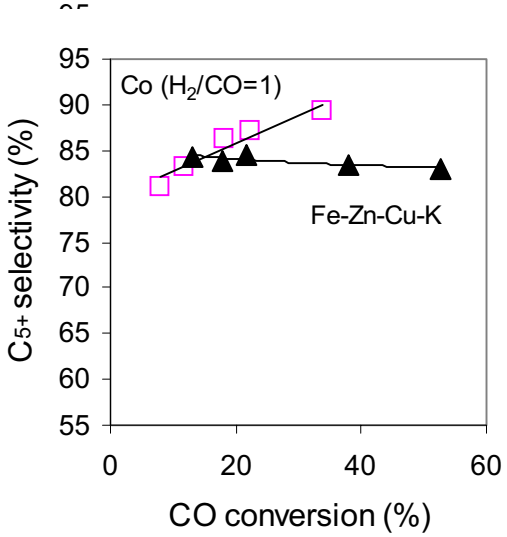

Figure 26. C_{5+} selectivity as a function of CO conversion at 220°C on Co/SiO_2 ($H_2/CO=1$, 43.6 atm), and Fe-Zn-Cu-K ($H_2/CO=2$, 31.6 atm).

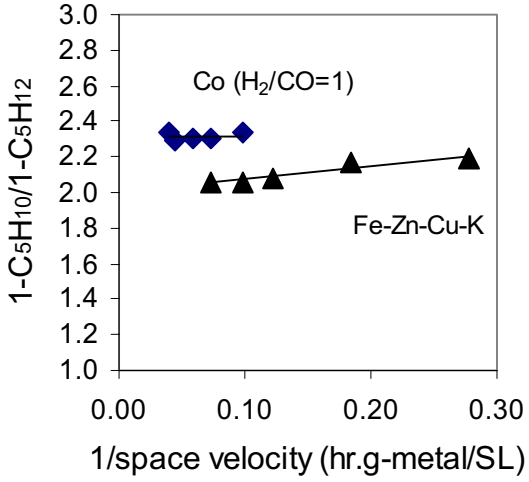

Figure 27. *1*-C_5H_{10}/*n*-C_5H_{12} selectivity as a function of reciprocal space velocity at 220°C on Co/SiO_2 ($H_2/CO=1$, 43.6 atm), and Fe-Zn-Cu-K ($H_2/CO=2$, 31.6 atm).

Since the surface CO*/H* ratio is enhanced by operation of the reaction at a H_2/CO ratio of 1 instead of 2, the Co surface appears to be less hydrogenating (Figure 27). While it has been observed in earlier quarters that the Co/SiO_2 catalyst promotes secondary hydrogenation reactions at 200°C and a H_2/CO ratio of 2, no secondary hydrogenation is observed as evidenced by the zero slope of the *1*-pentene/*n*-pentane curve. Flory plots for the Co catalyst at the two H_2/CO ratios at 200°C and 220°C are shown in Figure 28. A decrease in the H_2/CO ratio from 2 to 1 leads to unchanged Flory plots at a given reaction temperature, indicating that secondary chain growth by readsorption of olefins is unaffected by this increased CO coverage on the catalyst. However, at 220°C, the chain growth probability at higher carbon numbers appears to decrease which can be explained by the ease of desorption of α-olefins with increasing temperature and their subsequent non-participation in secondary chain growth reactions.

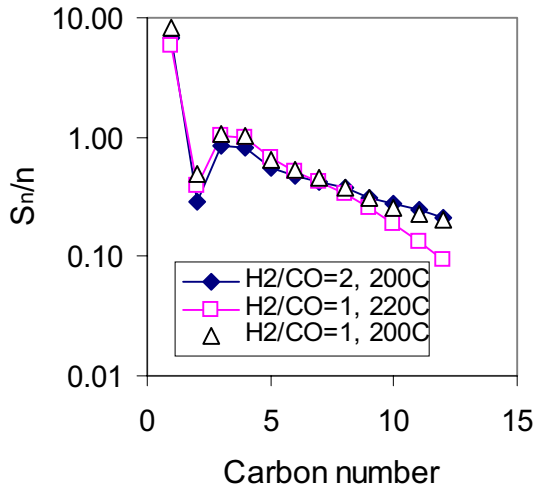

Figure 28. Flory plots for a 21.9% Co/SiO_2 catalyst at: 1) H_2/CO=2, 20 atm, 200°C, 2) H_2/CO=1, 43.6 atm, 220°C, and 3) H_2/CO=1, 43.6 atm, 200°C.

2. Effect of reaction pressure on the behavior of Co/SiO_2 for FTS reactions

During the previous quarter, FTS reaction was also conducted with a 21.9% Co/SiO_2 catalyst at different reaction pressure. This was done in anticipation of a series of for *in situ* FTIR spectroscopic experiments that will be carried out in the next quarter in order to study the autocatalytic water effects. Due to the pressure limitations of the transmission FTIR cell, fixed-bed reactor experiments were conducted at 200°C and 5 atm to study the FTS kinetics on the Co/SiO_2 catalyst under these conditions as well as to verify the existence of the autocatalytic water effect at these low pressures.

The Co site-time yields obtained on the 21.9% Co/SiO_2 catalyst at 5 atm and 20 atm are shown as function of the average water mole fraction in the reactor in Figure 29. The empty symbols represent data points corresponding to space velocity runs whereas the filled symbols represent water addition data. The site-time yields are similar at both

pressures and increase with increasing H_2O concentration as observed before confirming the existence of water effect even at low pressures [19-21,25]. Similarly the CH_4 and C_{5+} selectivities also are affected by water in both cases (Figures 30 and 31).

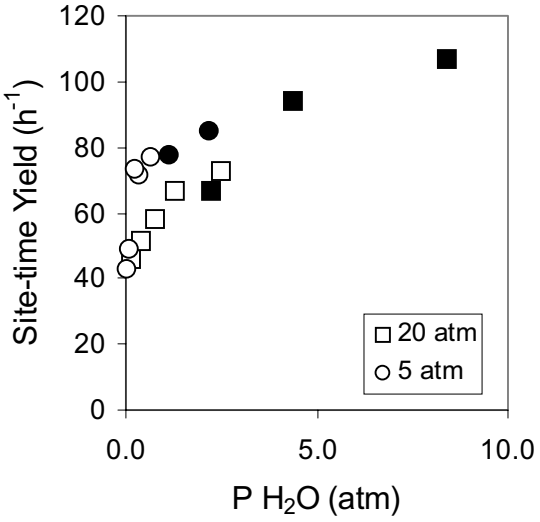

Figure 29. Co site-time yield as a function of average mole fraction of H_2O on a 21.9% Co/SiO_2 catalyst at 200°C; Empty symbols: Space velocity runs, Filled symbols: Water addition runs.

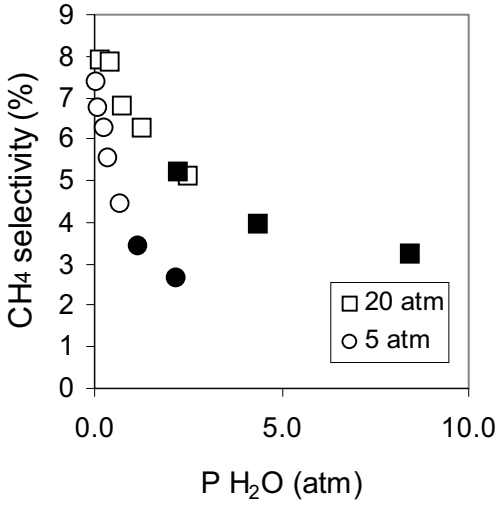

Figure 30. CH_4 selectivity as a function of average mole fraction of H_2O on a 21.9% Co/SiO_2 catalyst at 200°C; Empty symbols: Space velocity runs, Filled symbols: Water addition runs.

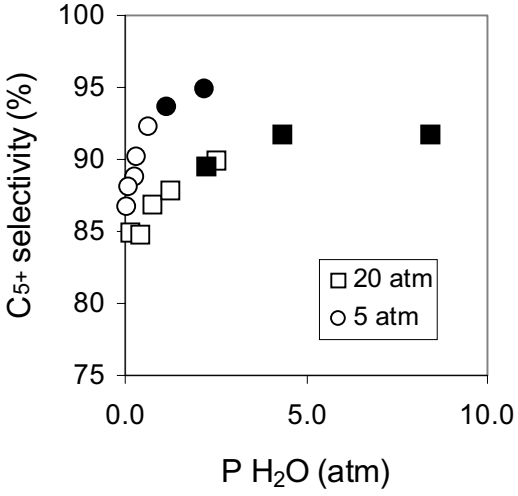

Figure 31. C_{5+} selectivity as a function of average mole fraction of H_2O on a 21.9% Co/SiO_2 catalyst at 200°C; Empty symbols: Space velocity runs, Filled symbols: Water addition runs.

Since our low-pressure FTS reaction studies have shown the existence of the water effect, this condition will be used for the *in situ* FTIR spectroscopic experiments with Co/SiO_2 both with and without the addition of water. The IR spectrometer has been relocated to a different unit and modifications are being done in order to carry out high-pressure experiments with the transmission IR cell. These studies are expected to be completed in the upcoming quarter.

II. APPENDIX
1. References

1. M. E. Dry, The Fisher-Tropsch Synthesis, in *Catalysis-Science and Technology*, Vol. 1, p. 160, J. R. Anderson and M. Boudart eds., Springer Verlag, New York, 1981.
2. F. Fischer and H. Tropsch, *Brennstoff-Chem.* 7 (1926) 97.
3. R. B. Anderson, in *Catalysis* Vol. 4, p. 29, P. H. Emmett eds., Van Nostrand-Reinhold, New York, 1956.
4. H. H. Storch, N. Golumbic and R. B. Anderson, *The Fischer-Tropsch and Related Syntheses*, Wiley, New York, 1951; R. B. Anderson, *The Fischer-Tropsch Synthesis*, Wiley, New York, 1984.
5. H. Kolbel and M. Ralek, *Catal. Rev.-Sci. Eng.* 21 (1980) 225.
6. J. W. Niemantsverdriet and A. M. van der Kraan, *J. Catal.* 72 (1981) 385.
7. J. A. Amelse, J. B. Butt and L. J. Schwartz, *J. Phys. Chem.* 82 (1978) 558.
8. G. B. Raupp and W. N. Delgass, *J. Catal.* 58 (1979) 348.
9. R. Dictor and A. T. Bell, *J. Catal.* 97 (1986) 121.
10. J. P. Reymond, P. Meriaudeau and S. J. Teichner, *J. Catal.* 75 (1982) 39.
11. C. S. Kuivila, P. C. Stair and J. B. Butt, *J. Catal.* 118 (1989) 299.
12. C. S. Huang, L. Xu and B. H. Davis, *Fuel Sci. Tech. Int.* 11 (1993) 639.
13. S. Soled, E. Iglesia and R. A. Fiato, *Catal. Lett.* 7 (1990) 271.
14. S. Soled, E. Iglesia, S. Miseo, B. A. DeRites and R. A. Fiato, *Topics in Catal.* 2 (1995) 193.
15. E. Iglesia, A research proposal submitted to the Division of Fossil Energy.
16. R. J. O'Brien, L. Xu. R. L. Spicer and B. H. Davis, *Energy and Fuels*, 10 (1996) 921.
17. D. B. Bukur, D. Mukesh, and S. A. Patel, *Ind. Eng. Chem. Res*., 29, 194 (1990).
18. 1st Quarterly report, 1999. U.S. Department of Energy under contract # DE-FC26-98FT40308.
19. 2nd Quarterly report, 1999. U.S. Department of Energy under contract # DE-FC26-98FT40308.
20. 3rd Quarterly report, 1999. U.S. Department of Energy under contract # DE-FC26-98FT40308.
21. 4th Quarterly report, 1999. U.S. Department of Energy under contract # DE-FC26-98FT40308.
22. 1st Quarterly report, 2000. U.S. Department of Energy under contract # DE-FC26-98FT40308.
23. 2nd Quarterly report, 2000. U.S. Department of Energy under contract # DE-FC26-98FT40308.
24. 3rd Quarterly report, 2000. U.S. Department of Energy under contract # DE-FC26-98FT40308.
25. E. Iglesia, *Appl. Catal. A*, 161 (1997) 59.
26. E. Iglesia, S.C. Reyes, R.J. Madon, and S.L. Soled, *Advances in Catal*., 39 (1993) 221.
27. D.O. Uner,, M. Pruski, and T.S. King, *Topics in Catal.*, 2 (1995) 59.
28. R.A. Dalla Betta, and M. Shelef, *J. Catal*., 48 (1977) 111.
29. C.S. Kellner, and A.T. Bell, *J.Catal*., 70 (1981) 418.
30. E. Iglesia, S.L. Soled, R.A. Fiato, and G.H. Via, *J. Catal.*, 143 (1993) 345.

Task 12. Reporting/Project Management

Four monthly and one quarterly reports have been completed.